NASA TECHNICAL NOTE

NASA TN D-6187

A STUDY OF THE HARTREE-FOCK MODEL SPACE FOR LIGHT DEFORMED NUCLEI

by William F. Ford, Richard C. Braley,
and J. Bar-Touv

Lewis Research Center
Cleveland, Ohio 44135

NATIONAL AERONAUTICS AND SPACE ADMINISTRATION • WASHINGTON, D. C. • MARCH 1971

1. Report No. NASA TN D-6187	2. Government Accession No.	3. Recipient's Catalog No.

4. Title and Subtitle	5. Report Date
A STUDY OF THE HARTREE-FOCK MODEL SPACE FOR LIGHT DEFORMED NUCLEI	March 1971
	6. Performing Organization Code

7. Author(s) William F. Ford, Richard C. Braley, Lewis Research Center; and J. Bar-Touv, Negev Univ., Beer-Sheva, Israel	8. Performing Organization Report No. E-5941

9. Performing Organization Name and Address	10. Work Unit No. 129-02
Lewis Research Center National Aeronautics and Space Administration Cleveland, Ohio 44135	11. Contract or Grant No.
	13. Type of Report and Period Covered

12. Sponsoring Agency Name and Address	Technical Note
National Aeronautics and Space Administration Washington, D.C. 20546	14. Sponsoring Agency Code

15. Supplementary Notes

16. Abstract

A systematic investigation is made of the effects of altering the truncated basis space used in deformed Hartree-Fock studies of light nuclei. Both the number of basis functions and their radial dependence are varied; the latter is accomplished by changing the oscillator parameter or by using Wood-Saxon eigenfunctions. From a study of properties both of the intrinsic Hartree-Fock state and the physical states projected from it, we concluded that present results are too sensitive to alterations in the basis space to provide a meaningful test of the model.

17. Key Words (Suggested by Author(s))	18. Distribution Statement
Nuclear structure Inelastic scattering Hartree-Fock model	Unclassified - unlimited

19. Security Classif. (of this report)	20. Security Classif. (of this page)	21. No. of Pages	22. Price*
Unclassified	Unclassified	46	$3.00

A STUDY OF THE HARTREE-FOCK MODEL SPACE FOR

LIGHT DEFORMED NUCLEI

by William F. Ford, Richard C. Braley,
and J. Bar-Touv*

Lewis Research Center

SUMMARY

The deformed Hartree-Fock method is used to study the effect on various nuclear properties of altering the truncated basis space used in structure calculations. After a brief discussion of the Hartree-Fock model and the means by which nuclear properties are obtained from the projected physical states, results are presented for the nuclei neon-20, magnesium-24, silicon-28, and sulfur-32. Intrinsic spectra, nuclear radii, electromagnetic transition rates, electron scattering form factors, and inelastic proton scattering cross sections are investigated and wherever possible compared with experiment. Calculations are performed with both Wood-Saxon and harmonic oscillator basis functions; 6 Wood-Saxon functions are used, and up to 15 harmonic oscillator functions with various values of the oscillator length. Results show that changes in the basis space produce rather dramatic changes in the nuclear properties, indicating that Hartree-Fock calculations of the type presented here are being performed in an inadequate basis space.

INTRODUCTION

The shell model and many of its ensuing developments have established that a microscopic description of the nucleus, in terms of the motions of individual nucleons, can be successfully used to predict energies, spins, and parities of the low-lying nuclear states (refs. 1 to 3). While such descriptions are generally designed to study level systematics, the wave functions so obtained have occasionally been subjected to more rigorous tests, such as prediction of electromagnetic transition rates (refs. 4 to 6), electron scattering form factors (refs. 7 and 8), and inelastic proton scattering cross sections

---

*Professor of Physics, Negev University, Beer-Sheva, Israel.

(refs. 9 to 11). Most of these properties are quite sensitive to the behavior of the wave function in the vicinity of the nuclear surface, whereas energy level systematics are thought to be more dependent on details within the nuclear interior. Calculations of surface-dependent properties have been, for the most part, less successful in reproducing experimental data.

In recent years the number of such microscopic investigations has steadily increased. These studies differ from one another mainly in the type of two-body interaction employed and in the size of the model space. The interaction may be designed to fit the nucleon-nucleon scattering data (ref. 12), may be of the renormalized or "effective" type (ref. 13), or may be obtained from an approximate solution of the Bethe-Goldstone equation (refs. 14 and 15). The model space nearly always employs harmonic oscillator wave functions, but there is little uniformity in the choice of oscillator length. Enough functions are included to allow for configuration mixing or deformation of orbits; for the heavier nuclei, calculations are often kept within reasonable bounds by presuming the existence of an inert, closed-shell core.

Efforts to extend the early shell model calculations have been devoted primarily to spherical vibrational nuclei, with correlations between nucleons moving in an average field being introduced via pairing (ref. 2). Excited states of these nuclei can be obtained by using some form of the random-phase approximation (refs. 2 and 3).

At the same time there has been significant progress in our understanding of deformed rotational nuclei. Here the chief means of investigation has been the Hartree-Fock (HF) method, which has received its greatest attention in the study of light deformed nuclei. One of the major advantages of working with light nuclei is that the inert closed-shell core assumption can be dropped and the problem is still tractable with respect to projection of states of good angular momentum from the intrinsic HF wave functions.

Recent calculations by several groups indicate that the HF method (or HF with slight variations) provides a good description of low-lying states of the light deformed nuclei (refs. 1, 16 to 18). In most of the nuclei studied it was found that the correct level ordering was reproduced, with the level spacings in good agreement with experiment (refs. 5, 16, 17, and 19). On the other hand, E2 rates and inelastic proton cross sections obtained from projected HF states indicate that these functions do not have the proper behavior needed to predict correctly the magnitudes of quantities associated with inelastic transitions. If the underlying assumption of the HF method is correct, namely, that excited levels within a band are generated from the same intrinsic state, then the source of the difficulty may well be the asymptotic form of the intrinsic HF state itself.

Most HF calculations have made use of basis functions with harmonic oscillator radial dependence, in spite of their rapid fall-off at large distances. Of course, if a sufficiently large number of such states were included, the correct asymptotic behavior could be produced. Indeed, recent studies by several groups indicate that calculated

2

nuclear properties improve - relative to experiment - as the size of the model space increases. Bassichis, Pohl, and Kerman (ref. 20) have studied the intrinsic HF state using both four and six major shells. They found that the quadrupole moment is quite sensitive to extension of the space, while the binding energy, rms radius, and kinetic energy per particle apparently are not. Gunye (ref. 5) examined projected energies for several nuclei in the lower half of the 2s-1d shell and found the spectra improved considerably as the space was enlarged to include four major shells. Preliminary investigations by the present authors (refs. 21 and 22) revealed that E2 rates and inelastic proton cross sections obtained from projected HF wave functions are substantially affected by the number and kind of basis functions used. These findings provide ample justification for further study of the effect on HF calculations of variations in the model space, particularly with regard to inelastic transitions induced by scattering or interaction with the electromagnetic field.

Microscopic descriptions of inelastic nucleon scattering have received considerable attention in recent years (refs. 9 to 11) largely as a result of advances in the theory of nuclear structure. Most applications have been to nuclei in the collective vibrational or rotational regions where a large number of structure calculations have been made. The distorted wave Born approximation (DWBA) is generally used to describe the scattering process, and the structure problem is solved with an inert core. Exceptions include coupled channel calculations by Glendenning (ref. 11) (but with an inert core) and DWBA studies by the present authors (ref. 9) in which core effects are explicitly treated. There are indications that DWBA may be adequate for low-lying states in most of the light deformed nuclei, but that coupled channels will be required for states with higher excitation energy.

The scattering of high-energy electrons from nuclei also provides a powerful tool for nuclear structure studies. As a means by which nuclear models may be tested, electron scattering has the attractive feature that the electron-nucleus interaction is well understood. This is in contrast to the situation in nucleon scattering, where uncertainties in the nuclear model are further complicated by lack of knowledge of the nucleon-nucleus force.

The analysis of high-energy electron scattering is carried out most easily in the first Born approximation; however, it is well known that this method is inadequate for large momentum transfers and that zeros occur at the diffraction minima. Baker (ref. 23) has proposed an approximation for high-energy electron scattering based on the eikonal approach developed by Glauber (ref. 24). Baker's high-energy approximation fills in the zeros of the diffraction minima and agrees well with the results of phase shift analyses. To our knowledge, however, this technique has only been tested for the simplest nuclear models.

There is a large amount of experimental data available for the 2s-1d shell nuclei. As a result of this, together with evidence that many of these nuclei have deformed

equilibrium shapes, the 2s-1d shell has become a testing ground for the deformed HF method. Of the nuclei in this region, neon-20 (^{20}Ne), magnesium-24 (^{24}Mg), silicon-28 (^{28}Si), and sulfur-32 (^{32}S) have received the greatest attention because of their convenient symmetries (even-even, N = Z). While it is generally conceded that the simple HF model (i. e., a single Slater determinant for the intrinsic state) provides a fairly good description of ^{20}Ne and ^{24}Mg, the simple model appears to be inadequate for ^{28}Si and ^{32}S. Accordingly there have been several attempts to explain their structure in terms of slight modifications of the HF method (refs. 16, 17, and 25). Among these, Bar-Touv and Goswami have proposed a model of "inverted coexistence" which seems to be promising (ref. 25). It remains now to make microscopic studies of these nuclei with extended model spaces.

The purpose of this work is to examine, as consistently as possible, the effect of alterations in the model space on nuclear properties predicted by the Hartree-Fock method. Wave functions are obtained by projecting states of good angular momentum from intrinsic HF states. Several nuclear properties are examined for model spaces of different size and with Wood-Saxon radial dependence as well as the usual harmonic oscillator behavior.

For the comparison of Wood-Saxon and harmonic oscillator cases only six basis functions are used, since all the other Wood-Saxon eigenfunctions are unbound. In this case the severe truncation makes it necessary to use an "effective" nucleon-nucleon interaction, and the Volkov force (ref. 26) was chosen. For the comparison of model-space size, sets of 6, 10, and 15 harmonic oscillator functions are used with varying oscillator lengths. Here one of the "realistic" nucleon-nucleon interactions, namely, that devised some years ago by Tabakin (ref. 27), is used.

In the next section, a brief review of the HF method is given, and a summary of the technique used to calculate nuclear properties from the projected wave functions. Details of the calculation are outlined, the results are discussed, and a summary and some conclusions are presented in later sections.

THEORY

Nuclear States

The low-energy spectra of some nuclei remind one of the spectrum of a rigid rotator, that is, the energy levels are proportional to $J(J + 1)$. This observation led to the early descriptions of deformed nuclei in terms of a rotating intrinsic state (ref. 28). Thus, a natural starting point for the deformed HF method was provided. In the HF picture, the intrinsic state is described in terms of nucleons moving in a deformed field with respect to body-fixed axes. Physical states of the system may be thought of in

terms of various rotations of the intrinsic state. Formally, the physical states may be obtained from the intrinsic state by the well-known method of angular momentum projection (ref. 29).

Intrinsic states. - In the HF method the intrinsic nuclear wave function is approximated by a single Slater determinant

$$\Phi_K = (A!)^{-1/2} \det\{\varphi_\lambda(\vec{x}_n)\} \tag{1}$$

whose orbitals $\varphi_\lambda(\vec{x}_n)$ are determined by minimizing the expectation value of the intrinsic nuclear Hamiltonian. Solution of this variational problem leads to the HF equations

$$h|\lambda\rangle = e_\lambda|\lambda\rangle \tag{2a}$$

where

$$\langle i|h|j\rangle = \langle i|t|j\rangle + \sum_\lambda \langle i\lambda|V|\widetilde{j\lambda}\rangle \tag{2b}$$

The i and j refer to single-particle (s.p.) states, and the sum on λ runs overall occupied orbits. In equation (2b), t represents the s.p. kinetic energy operator, and the tilde indicates that the two-body matrix elements are antisymmetrized.

To solve the HF equations, each of the orbits is written in the form of a (truncated) expansion

$$|\lambda\rangle = \sum_j C_j^\lambda|j\rangle \tag{3}$$

in which the summation over j is partly restricted by the symmetries of the nuclear system. The C_j^λ are determined self-consistently from equations (2), and the HF energy is then found from the expression

$$E_{HF} = \frac{1}{2} \sum_\mu \left[\langle\mu|t|\mu\rangle + e_\mu\right] \tag{4}$$

Physical states. - The intrinsic state Φ_K obtained from the solution of the HF equations is not an eigenfunction of total angular momentum. However, there is a well-known prescription for obtaining such eigenfunctions, namely (refs. 1 and 29),

$$\psi_{JM}(1, \ldots, A) = \frac{2J+1}{8\pi^2} \int d\Omega \ D^J_{MK}(\Omega)^* R(\Omega) \Phi_K(1, \ldots, A) \tag{5}$$

where $D^J_{MK}(\Omega)$ is the rotation matrix, R is the rotation operator, and M and K are the projections of the total angular momentum J onto the space- and body-fixed axes, respectively. When the restriction to axial symmetry is made on the HF state, equation (5) simplifies to

$$\psi_{JM}(1, \ldots, A) = \frac{2J+1}{2} \int_0^{\pi} \sin\theta \ d\theta \ d^J_{MK}(\theta) e^{-i\theta J_y} \Phi_K(1, \ldots, A) \tag{6}$$

where $d^J_{MK}(\theta)$ is the reduced rotation matrix. In all of the analysis which follows the nuclei to be considered have even N and even Z, and only states within the ground state rotational band are considered (i. e., $K = 0$). Consideration of the symmetries of Φ_K enables one to show that, for even-even nuclei, the J values of states in the ground state band are all even.

Nuclear Properties

The prediction of nuclear properties requires evaluation of reduced matrix elements of certain operators between initial and final states of the nucleus. Most of these operators can be expressed as a sum of single-particle operators (an exception, of course, being the nuclear Hamiltonian). When this is the case, it is possible to evaluate the reduced matrix elements in such a way that the integration over the coordinates of the single-particle operator is the last to be performed. The previous integrations over the other (A-1) coordinates thus yield a quantity which depends only on the initial and final states of the nucleus and the nature of the transition involved. This leads directly to the concept of an inelastic transition density $\rho^{if}_{LSJ}(r)$, which essentially gives, for the transition $i \rightarrow f$, the probability for absorption of angular momentum $\vec{J} = \vec{L} + \vec{S}$ by the last nucleon as a function of its distance from the nuclear origin. This very useful concept has been discussed in detail in a previous publication (ref. 30).

In the cases considered here, each single-particle operator Ω may be expanded in terms of spin-angle tensors with coefficients $\omega_{LSJ}(r)$ which give the radial dependence of the operator. Reduced matrix elements of the many-body operator may then be expressed as

$$\left\langle J_f \left\| \sum_{n=1}^{A} \Omega(n) \right\| J_i \right\rangle_J = \sum_{LS} \int_0^\infty \rho_{LSJ}^{if}(r)\omega_{LSJ}(r)r^2 \, dr \tag{7}$$

The expansion of $\rho_{LSJ}^{if}(r)$ in terms of a biorthogonal set of (Gauss-Laguerre) functions is particularly convenient from a calculational point of view since it enables one to re-express equation (7) as

$$\langle J_f \| \Omega \| J_i \rangle = \sum_{LS} \sum_{n=0}^{\infty} \rho_{LSJn}^{if} \int_0^\infty \omega_{LSJ}(r)\widetilde{\mathscr{F}}_{nL}(\alpha, \beta r)r^2 \, dr \tag{8}$$

For most operators the integral over r can be carried out analytically, and the sum over n has been found to converge rapidly. This is accomplished by suitable choice of the adjustable parameters α and β appearing in the Gauss-Laguerre functions.

Static nuclear properties. - The initial and final states of the nucleus are the same in this case. For ground state properties of even-even nuclei, the calculation of the matrix elements is particularly simple since $J_i = J_f = 0$ and $L = S = J = 0$. One of the ground state properties which we require to be in agreement with experiment is the rms radius. In this case, the operator is

$$R^2 = \frac{1}{A} \sum_{n=1}^{A} r_n^2 \tag{9}$$

and equation (8) becomes

$$\langle i \| R^2 \| i \rangle = \frac{\sqrt{4\pi}}{A\beta^2} (1 - \alpha)^{-5/2} \sum_{n=0}^{\infty} \left(\frac{n}{\alpha} + \frac{3}{2} \right) \widetilde{\rho}_{000n}^{ii} \tag{10}$$

where, for convenience, we have introduced

$$\widetilde{\rho}_{LSJn}^{if} \equiv \left(\frac{\alpha}{\alpha - 1} \right)^n \rho_{LSJn}^{if} \tag{11}$$

The electric quadrupole moment provides information about the shape of the nucleus. To obtain it we evaluate the reduced matrix element of

$$Q_2 = e\left(\frac{16\pi}{5}\right)^{1/2} \sum_{i=1}^{A} r_i^2 Y_2^0(\hat{r}_i) \frac{1 + \tau_i}{2} \qquad (12)$$

where τ_n is the z-component of the isotopic spin operator for the nth nucleon. The result is

$$\langle J_f \| Q_2 \| J_f \rangle = e\left(\frac{16\pi}{5}\right)^{1/2} \beta^{-2}(1 - \alpha)^{-7/2} \sum_{n=0}^{\infty} \tilde{\rho}_{202n}^{ffp} \qquad (13)$$

Only the proton part of the transition density is involved here, as is indicated by the p superscript on $\tilde{\rho}$.

As pointed out in the INTRODUCTION, the elastic scattering of high-energy electrons is described more accurately by the Baker approximation than by the first Born approximation. The form factor for electron scattering is given by

$$|F(q)|^2 = \frac{\dfrac{d\sigma}{d\Omega}}{\left(\dfrac{d\sigma}{d\Omega}\right)_M} \qquad (14)$$

in which $(d\sigma/d\Omega)_M$ is the Mott cross section and

$$\frac{d\sigma}{d\Omega} = |M|^2$$

where

$$M = \frac{k}{i} \int_0^\infty J_0(qb)\left[e^{i\chi(b)} - 1\right] b \, db \qquad (15)$$

as shown by Baker. When microscopic wave functions are used to represent the target, the evaluation of equation (15) is rather involved; it is presented in the appendix.

Dynamic nuclear properties. - The prediction of quantities which involve transitions to excited states provides a more sensitive test of the validity of any nuclear model. Of particular interest to us shall be electromagnetic transition rates and inelastic particle scattering. For the Eλ transition rate from i to f we obtain (ref. 30)

$$B(E\lambda; \; i \to f) = e^2 \frac{2J_f + 1}{2J_i + 1} \left| \beta^{-\lambda}(1 - \alpha)^{-\lambda-(3/2)} \sum_{n=0}^{\infty} \tilde{\rho}_{\lambda o\lambda n}^{ifp} \right|^2 \tag{16}$$

For the inelastic scattering of high-energy electrons we evaluate the Born approximation to the electron scattering form factor, obtaining an expression of the form

$$\left| F(q) \right|^2 = \frac{2J_i + 1}{2J_i + 1} \sum_L \left| G_L \sum_{n=0}^{\infty} \tilde{\rho}_{LoLn}^{ifp} \tilde{\mathscr{F}}_{nL}(1 - \alpha', \gamma'q) \right|^2 \tag{17}$$

Details of the derivation may be found in reference 30.

For the inelastic scattering of protons it is necessary, as mentioned in the INTRO-DUCTION, to make some assumptions concerning the nature of the nucleon-nucleus force responsible for the transition. The standard assumption, and the one adopted here, is that this interaction may be represented as a sum of two-body "effective" potentials:

$$V(\vec{x}_o, \vec{A}) = \sum_{n=1}^{A} V(\vec{x}_o, \vec{x}_n) \tag{18}$$

In order to calculate the scattering amplitude, the reduced matrix elements of $V(\vec{x}_o, \vec{A})$ must be obtained as functions of the projectile coordinates $\vec{x}_o$, and then expanded in spin-angle tensors; the radial coefficients $f_{LSJ}^{if}(r_o)$ are known as the nucleon scattering form factors (ref. 9). Because of the above assumption, V is a one-body operator in the coordinates of the target nucleons and the methods of equations (7) and (8) apply. The resulting form factors are expressible as

$$f_{LSJ}^{if}(r_o) = \sum_{N=0}^{\infty} f_{LSJN}^{if} \tilde{\mathscr{F}}_{NL}(0, \zeta r_o)$$

For details the reader is again referred to reference 30.

DETAILS OF THE CALCULATIONS

The HF variational problem was solved subject to the condition that the intrinsic state possess axial symmetry and fourfold degeneracy (ref. 1). Each orbit is therefore specified by its z-components of spin and isospin and further specified by its projections

onto basis functions labeled by the quantum numbers $(n\ell j)$. The model spaces to be used in this work are listed in table I.

The final choice of oscillator length $b = \sqrt{\hbar/M\omega}$ for the harmonic oscillator functions is based on the requirement that the rms radius be well reproduced for each nucleus, that is, the rms radius serves as a constraint in the variational problem. However, the effect (on other quantities) of variation of the oscillator length is also investigated.

The parameters of the potential which produced the Wood-Saxon functions were chosen so as to yield approximately the O^{17} experimental single-particle energies (ref. 4). This potential has the form

$$V(r) = V_0 \rho(r) - \alpha V_0 \left(\frac{\hbar}{2Mc}\right)^2 \frac{\vec{\sigma \ell}}{r} \frac{d}{dr} \rho(r)$$

with

$$\rho(r) = \left[1 + \exp\left(\frac{r - R}{a}\right)\right]^{-1}$$

and V_O = -56.5 MeV, R = 3.15 femtometers, a = 0.65 femtometer, and α = 20. There are states generated by this potential other than those shown in table I, but these lie in the continuum.

The two-body matrix elements have been calculated using the Tabakin interaction for most of the cases in which harmonic oscillator functions are used. This is a smooth, nonlocal separable potential which has been used successfully in several shell model and HF studies (refs. 12 and 20). The general form of the potential is

$$V(\vec{r}, \vec{r}') = \frac{\hbar^2}{m} \sum_{\substack{\alpha M \\ \ell \ell'}} \{S_{\alpha \ell \ell'} g_{\alpha \ell}(r) g_{\alpha \ell'}(r') + t_{\alpha \ell \ell'} h_{\alpha \ell}(r) h_{\alpha \ell'}(r')\} Y_{\alpha \ell}^M(\hat{r}) Y_{\alpha \ell'}^M(\hat{r}')$$

details may be found in reference 12.

For calculations involving the comparison of Wood-Saxon and harmonic oscillator functions, one of the "effective" nucleon-nucleon interactions was used, as mentioned in the INTRODUCTION. We have chosen a Volkov force (ref. 26) which yields fairly good saturation properties for the p-shell nuclei:

$$V(|\vec{r}_1 - \vec{r}_2|) = \{\alpha + \beta \vec{\sigma}_1 \cdot \vec{\sigma}_2 + \gamma \vec{\tau}_1 \cdot \vec{\tau}_2 + \delta \vec{\sigma}_1 \cdot \vec{\sigma}_2 \vec{\tau}_1 \cdot \vec{\tau}_2\} f(|\vec{r}_1 - \vec{r}_2|)$$

where

$$f(|\vec{r}_1 - \vec{r}_2|) = -78\ e^{-(|\vec{r}_1-\vec{r}_2|^2)/2.25} + 82.5\ e^{-(|\vec{r}_1-\vec{r}_2|^2)/0.64}$$

with $\alpha = 0.1875$, $\beta = -0.0775$, $\gamma = 0.2025$, and $\delta = -0.1775$. Another reason for the choice of this potential is that it is local, which is particularly convenient for calculating two-body matrix elements with Wood-Saxon wave functions using the technique of reference 4.

Transition amplitudes for inelastic proton scattering are obtained in the DWBA, neglecting exchange effects between projectile and target nucleons. The following optical potential is used to generate the distorted waves:

$$U(r) = V_c(r) - V_0 \rho_V(r) - \frac{4i}{a_s} W_s \rho_s(r) - V_{LS}\left(\frac{\hbar}{m_\pi c}\right)^2 \frac{\vec{\sigma}\vec{l}}{a_{LS}r} \rho_{LS}(r)$$

where V_c is the Coulomb term, V_0 the strength of the real potential, W_s the strength of the surface absorption, and V_{LS} the spin-orbit strength. The quantity $\rho_V(r)$ is the usual Wood-Saxon form factor, and ρ_S and ρ_{LS} are derivatives of functions similar to ρ_V but with appropriate radius and diffuseness parameters.

Two different forms of the interaction between projectile and target nucleon are considered, the first due to Glendenning and Veneroni (ref. 10):

$$V(r_{12}) = -52\ e^{-(r_{12}/1.85)^2}(P_{TE} + 0.6\ P_{SE})$$

and the second (with a considerably shorter range) to Thompson and Tang (ref. 31):

$$V(r_{12}) = -72.98\ e^{-(r_{12}/1.47)^2}(P_{TE} + 0.632\ P_{SE})$$

RESULTS

Harmonic Oscillator Basis

In the usual structure calculation which employs harmonic oscillator basis functions, the number of functions to be included and the value of the oscillator length are "free parameters." Although the effect of enlarging the model space has been investigated in

some detail, the effect of variations in the oscillator length has not been studied extensively. When a truncated basis is employed, however, the results will depend on the oscillator length used, and the nature of this dependence should be examined.

In this section we present results indicating the effect on various nuclear properties of varying both the number of basis functions and the value of the oscillator length. In the final analysis, the oscillator length is adjusted so that the rms radius for each nucleus, calculated in the largest model space, is in agreement with experiment.

Neon-20. - We begin by presenting results for fixed oscillator length. In table II(a) are compared the intrinsic HF states and single-particle energies for the three model spaces defined in table I, using an oscillator length of 1.88 femtometers. In table II(b) the HF energies and gaps (between last occupied and first unoccupied orbitals) are also compared. The level ordering is preserved in all three cases, and the HF energy decreases (binding energy increases) as the model space is enlarged, as has been observed previously (ref. 20). The energy gap Δ increases as well, indicating that the HF solution becomes more stable as the model space is enlarged.

We now turn to the physical nuclear properties which are obtained by projecting states of good angular momentum from the intrinsic HF state. The projected energy spectrum for ^{20}Ne has been shown to improve as the model spacing is enlarged (ref. 5). However, other important nuclear properties have gone untested in this regard.

In table III we show the effect on the projected rms radius and E2 transition rate of variations in both the size of the model space and the value of the oscillator length. Table III(a) gives the results for fixed oscillator length. As the space is enlarged, the E2 rate increases, although even in the largest space it is far below the experimental value. On the other hand, the nucleus contracts as the number of basis functions is increased and eventually has a radius smaller than the experimental value. (Experimentally, $\langle R^2 \rangle^{1/2}$ = 2.79 fm, and B(E2; $0^+ - 2^+$) = 286 $e^2 \cdot$ fm^4. The error on $\langle R^2 \rangle^{1/2}$ is probably of the order of 5 percent. Experimental radii were obtained from R. de Swiniarski, and E2 rates appear in ref. 32.)

Table III(b) gives the results for a fixed number of basis functions, showing that as one might expect both the rms radius and the E2 rate increase with oscillator length. This is due to the displacement toward larger radius of the maxima of the radial functions as b is increased.

Finally, table III(c) shows the results when the rms radius is essentially fixed, serving as a constraint on the variational calculation. It should be noted that in none of these cases does the value of b minimize the HF energy, considered as a function of b. A typical example is shown in figure 1, where the HF energy is plotted as a function of oscillator length (for space 2). A smooth curve is drawn through the points indicating a minimum HF energy at b = 1.83 femtometers, whereas table III indicates that the correct rms radius is achieved at b = 1.88 femtometers.

As an additional test of the wave function, the E2 rates between other states within the ground state band are predicted and compared with experiment in table IV. The E2 rate for $4^+ \to 6^+$ is underestimated in much the same fashion as the $0^+ \to 2^+$ rate; however, the $2^+ \to 4^+$ rate is slightly beyond the experimental limit. It is surprising indeed to find a predicted E2 rate which overestimates the experimental result; in fact, in view of the experimental uncertainty in the rms radius, it is not unreasonable to claim agreement with experiment for this transition. Of course, the agreement may be fortuitous; but if not, the result suggests that perhaps each of the physical states should be generated from a different intrinsic state. Recent investigations by Castel and Parikh (ref. 16) indicate that this may be a better procedure than the standard approach, in which the idea of a band generated from a single Slater determinant is invoked.

Unfortunately, there are no experimental data available, at the present time, from which elastic electron scattering form factors for ^{20}Ne may be extracted. However, since the method developed by Baker has not been used previously to investigate microscopic nuclear wave functions, it seems worthwhile to display some of the changes which result from variations in the nuclear model and in the parameters which describe the scattering. In figure 2 the form factors are compared (for space 3 with $b = 1.93$ fm) in the Baker approximation and in the Born approximation. The more sophisticated method fills in the diffraction minimum and shifts the second maximum to lower q. Also shown is the result which occurs if correction is not made for the finite size of the proton. The effects of enlarging the model space are shown in figure 3; the trend is to shift the first minimum to larger q and to increase the magnitude for smaller q values.

We turn now to the case of inelastic proton scattering, recalling that the structure of the target nucleus as well as the radial dependence and mixture of the two-body force manifest themselves in the shape and size of the nuclear form factor. In figure 4 the scalar form factor $f_{202}^{if}(r)$ is presented for the $0^+ \to 2^+$ transition, using the Glendenning-Veneroni interaction. Although the shape of the form factor does not change noticeably, its magnitude increases with the number of basis functions. The vector form factor $f_{212}^{if}(r)$ has roughly the same shape as the scalar but is usually smaller by about two orders of magnitude.

The cross sections obtained using these form factors are shown in figure 5. As the model space is enlarged, the cross section nearly doubles, although its shape is not changed significantly. The angular distribution is given reasonably well; however, it underestimates the experimental data (of de Swiniarski) by at least a factor of 2 in the forward direction.

Since there are uncertainties in the interaction between the projectile and the bound nucleons, these calculations are repeated for the Tang force. As can be seen from the comparison in figure 6, the major difference in the form factors occurs for radii larger than 4 femtometers. The effect which this has on the cross section is shown in figure 7:

13

the magnitude of $d\sigma/d\Omega$ using the Glendenning-Veneroni force is generally larger than that using the Tang force, despite the fact that the latter is about 40 percent stronger. This occurs because of the short range of the Tang force, which makes the form factor smaller in the important surface region.

Magnesium-24. - The early HF studies of ^{24}Mg by Bar-Touv and Kelson indicated that the nucleus is asymmetric, because of the larger binding energy and gap possessed by the asymmetric solution. However, comparison of projected spectra for the two shapes (ref. 19), together with recent studies in which pairing effects are included (ref. 33), indicates that its intrinsic structure is still in doubt. Furthermore, Bar-Touv has observed that the symmetric and asymmetric states have a large overlap. For purposes of this study, therefore, there is little reason to prefer one solution to the other; the symmetric solution is actually chosen for convenience in projecting states of good angular momentum.

The intrinsic HF states and single-particle energies are compared in table V(a). (For brevity, results in the smallest space will not be presented for ^{24}Mg on the remaining nuclei.) The HF energies and gaps are shown in table V(b), and the variation of the HF energy with oscillator length in figure 8. The general trends are clearly the same as for ^{20}Ne, and we omit much of the detail; results for the ultimate choice of oscillator length are given in table V(c).

Some of the electromagnetic transition rates predicted are presented in table VI; the $0^+ \to 2^+$ rate is underestimated by about 25 percent, but as in the case of ^{20}Ne, the $2^+ \to 4^+$ is overestimated. It appears that the wave functions for both of these nuclei have similar inadequacies.

The electron scattering form factor is compared with unpublished experimental data of H. Hultzsch in figure 9. The predicted result is quite good for q-values up to 1.2 femtometer^{-1} but does not correctly predict the first minimum nor does it rise sufficiently at the secondary maximum. It is not clear whether this is due to the incorrect shape of the ^{24}Mg wave function in the nuclear interior or some inadequacy in the method for computing the form factor.

The DWBA prediction for inelastic proton scattering to the first 2^+ level is compared with experiment (ref. 34) in figure 10. The general quality of the predicted cross section is the same as for ^{20}Ne: the angular distribution is fairly good but drops off a little too rapidly at larger angles, and the prediction underestimates the data by roughly a factor of 2.

Silicon-28. - As mentioned in the INTRODUCTION, there are several reasons for suspecting that ^{28}Si is too complicated for description by the simple HF picture, and that one must resort to the more involved methods such as "inverted coexistence" or the inclusion of various other types of correlations. The projected energy spectrum yielded by the HF model is far too compressed, for one thing, and the $0^+ \to 2^+$ transition rate is badly underestimated.

14

On the other hand, all spectra and E2 rates calculated to date have made use of limited model spaces. Enlarging the model space is known to have a significant effect on these quantities, so there is still reason to study this nucleus in the simple HF picture. In the discussion of ^{28}Si, we will first examine the results obtained from the HF model, and then present some results based on the assumption of inverted coexistence.

The oblate solution of ^{28}Si is the lowest of the three (the other two being prolate, with $E_{HF} = -58.30$ MeV, and spherical, with $E_{HF} = -45.29$ MeV, for the largest space with $b = 2.09$ fm), and unless otherwise specified, will be the one for which results are given. In tables VII(a) and (b) the HF intrinsic states, HF energies, and energy gaps are compared for spaces 2 and 3. The general trends are similar to those for ^{20}Ne and ^{24}Mg. Results obtained when the oscillator length is varied are also quite similar and will be omitted for ^{28}Si and ^{32}S.

In table VII(c) one finds striking evidence, however, of the difference between ^{28}Si and the preceding nuclei. The ground state E2 rate is <u>overestimated</u> for both spaces, and <u>decreases</u> as the model space is enlarged. It is possible, of course, that this represents convergence toward the experimental value from above, much as the results for ^{20}Ne and ^{24}Mg seem to indicate convergence from below; however, the discrepancy between the measured $2^+ \rightarrow 4^+$ transition rate (60.1 e^2fm^4, $e = 1.6 \times 10^{-19}$ C) and the predicted value (193 e^2fm^4) is far greater than found for the previous nuclei. The electron scattering form factor is shown in figure 11, and the proton scattering cross section in figure 12. Although the quality of the former is about the same as found for ^{24}Mg, the drop in the proton cross section for angles smaller than 40° is discouraging. The overall impression is that ^{28}Si is not well described by the simple HF picture.

As mentioned earlier, there have been proposals for modifying the HF treatment of ^{28}Si. None of these has been tested using a detailed description in which the core orbitals are varied and an extended basis is used. The model of inverted coexistence (IC) proposed by Bar-Touv and Goswami (ref. 25) will be tested here. In this model, the 0_1^+ ground state and 0_2^+ excited state wave functions are taken to be linear combinations of the spherical and deformed (oblate) HF solutions:

$$\psi_1(0^+) = \alpha\Phi_S + \beta\Phi_D$$

$$\psi_2(0^+) = \alpha'\Phi_S + \beta'\Phi_D$$

The values of α and β are taken from the results of Bar-Touv and Goswami, and α' and β' are determined from the requirements of normalization and orthogonality.

In table VIII the predictions based on the IC model are compared with those predicted by the simple HF model and with experiment. With the IC model all three quantities are brought within the experimental limits. Unfortunately, the IC model has no

effect on the E2 rate for the $2^+ \to 4^+$ transition and negligible effect on the electron scattering form factor and inelastic proton cross section. (It should be noted that the proton scattering cross section might be changed considerably in a coupled channel calculation because of the strong coupling between the 2^+ and excited 0^+ states.)

Sulfur-32. - Generally the comments made previously with regard to ^{28}Si also apply to ^{32}S. The only specific exception to the introductory remarks is that early HF studies for this nucleus indicated that it might be asymmetric (ref. 35).

For ^{32}S, the prolate solution yields the lowest HF energy. Tables IX(a) and (b) compare the HF intrinsic states, HF energies, and energy gaps for this solution in spaces 2 and 3, with results very similar to those observed for ^{28}Si. The radius and E2 rate are compared in table IX(c), again with similar findings; the result for the oblate solution is also included because it is within the experimental limit (this is probably fortuitous). The qualitative features of the electron scattering form factor (fig. 13) and the inelastic proton scattering cross section (fig. 14) are much like those found for ^{28}Si.

An inverted coexistence calculation was not carried out for ^{32}S because of the accidental orthogonality of the prolate and spherical intrinsic states. (Our method for obtaining inelastic transition densities requires inversion of the matrix whose elements are the overlap integrals of the initial- and final-state orbits; because of the accidental orthogonality, the determinant of this matrix vanishes for the cross term.) We did carry out such a calculation for the oblate and spherical states, however, and found it yielded results analogous to those for a prolate-spherical ^{28}Si calculation. We suspect, therefore, that the IC model would probably fare no better for ^{32}S than it did for ^{28}Si.

Wood-Saxon Basis

In this section nuclear properties calculated using a Wood-Saxon basis are compared to those obtained with a corresponding harmonic oscillator basis. The choice of oscillator length (b = 1.924 fm) is based on previous investigations by two of the present authors (ref. 4), in which it was found that this value gave the best agreement between nuclear properties calculated using the two different bases when the core was inert.

The intrinsic HF states and single-particle energies for ^{20}Ne are compared in table X. The level ordering is the same for both bases, with the Wood-Saxon orbital energies slightly larger except for the last orbit. Similar results (not shown) are found for these intrinsic properties of the other three nuclei, except that in ^{32}S the ordering of the last three orbitals is different (they are nearly degenerate in the harmonic oscillator basis).

Table XI compares some other properties for the two bases, nucleus by nucleus. The WS prediction for the rms radius is always smaller than the HO prediction, and,

except for ^{32}S, closer to experiment. Since the Wood-Saxon well parameters were chosen so as to reproduce the ^{17}O single-particle energies, it is perhaps not surprising that the WS prediction should underestimate the nuclear size for heavier elements. The E2 rates are roughly comparable for all four nuclei. The HF energies (larger here because of the Volkov force) demonstrate an earlier (ref. 4) finding: because of the normalization to unity, the longer tails on the Wood-Saxon basis functions force them to be smaller within the nuclear interior, resulting in less binding energy.

A drawback of any study in which the well parameters do not change is illustrated in figures 15 and 16. In the former, the WS electron scattering form factor for ^{20}Ne is seen to be very similar to that obtained previously in the largest model space, while the HO form factor is quite poor; in figure 16, however, the reverse is true for ^{32}S.

Figure 17 demonstrates that the cross section for inelastic scattering of protons by ^{20}Ne is not significantly altered by the change in basis, except for a slight decrease in magnitude; the same holds true for the other three nuclei (not shown). Once again, it seems to be the combined action of normalization and the longer tail which is responsible for the decrease; the effect can be seen quite clearly in the ^{20}Ne form factors shown in figure 18.

CONCLUDING REMARKS

The purpose of this work has been to investigate the effects of alterations in the model space used for Hartree-Fock calculations. A number of different nuclear properties have been examined; these were obtained from microscopic wave functions of good angular momentum projected from the intrinsic HF states. The intrinsic states were assumed to have axial symmetry and fourfold degeneracy, but no inert core assumption was made. The 2s-1d shell nuclei ^{20}Ne, ^{24}Mg, ^{28}Si, and ^{32}S were chosen for this study because of their convenient symmetry properties and because of the large amount of experimental data available for them.

The general results indicate that the predicted nuclear properties vary significantly as the basis space is enlarged. These properties are likewise sensitive to the shape and extent of the radial basis functions. It was observed, for example, that if the correct nuclear radius is to be obtained, the oscillator length must vary significantly from nucleus to nucleus; similarly, the use of a (limited) Wood-Saxon basis requires different well parameters for different nuclei.

Even when a fairly large space was used in the structure study, it was found that, although ^{20}Ne and ^{24}Mg were described reasonably well by the simple HF picture, this was not true of the closed subshell nuclei ^{28}Si and ^{32}S. A test of the model of inverted coexistence for these nuclei seems to yield improved results for the ground state $0^+ \rightarrow 2^+$ transition rate and gives a good value for the excited state $0^+ \rightarrow 2^+$ transition rate; how-

ever, many other properties were unaffected by this modification, notably the other E2 rates, the electron scattering form factors, and the inelastic proton scattering cross sections.

Generally speaking, the electron scattering form factors predicted using the Baker approximation were unsatisfactory when compared with experiment. It is difficult to say whether this is due to poor nuclear wave functions or to inadequacy in the scattering approximation.

Some insight into this problem may be gained by comparing the nuclear densities (fig. 19) with the form factors (fig. 20) for the four nuclei. One expects in general to find a correlation between the smaller and larger portions of these curves, and vice versa, simply from the nature of the Fourier transformation which they represent. The slope of the form factor is directly proportional to R^2 as $q \to 0$, for instance, and the frequency of the form factor minima are closely associated with lack of smoothness in the density for small r.

But these curves demonstrate once again a correlation which is generally ignored, the correlation between asymptotic behavior and interior behavior resulting from the normalization condition. This illustrated rather dramatically in figure 19, where the reciprocal of the rms radius for each nucleus is marked along the scale at the right, to be compared with the nuclear density at the origin, which can be read from the scale at the left. The behavior of the density in the vicinity of the nuclear surface is evidently strongly correlated with its behavior at the origin.

Our major conclusion, of course, is that the Hartree-Fock model gives unreliable results if used in a model space as small as those examined here. This is unfortunate, for the simplicity of the scheme is lost as the model space is enlarged, to say nothing of the computing time.

On the other hand, we must point out other moderating conclusions. It is clear, for example, that the asymptotic part of the basis function plays an important role, and it may well be that the increase in the number of basis functions really represents an attempt to reproduce this asymptotic behavior. Therefore, no definitive statements about the size of the model space can be made until a study of this nature has been made with basis functions more appropriate to the problem.

Another question may be raised concerning the use of a "realistic" two-nucleon force rather than an "effective" one. With no evidence to the contrary to guide us, we made the assumption that the general trends would be the same in either case. The most accurate procedure would be to obtain solutions of the Bethe-Goldstone equation for each new basis set and then proceed to the HF problem; but such a task would be prohibitively difficult.

An alternative approach has been suggested recently (ref. 36). It is possible to develop the theory so that the operators contain the effect of the excluded space. This results, of course, in an effective interaction, but more importantly, it also results in

18

renormalized operators for all the observables studied here. At present the theory is in its preliminary stages but certainly should be considered in any future examination of model spaces for Hartree-Fock theory.

Lewis Research Center,
National Aeronautics and Space Administration,
Cleveland, Ohio, November 13, 1970,
129-02.

APPENDIX - THE BAKER APPROXIMATION

The high-energy approximation for electron scattering consists of using the approach of Glauber to solve the Dirac equation for an electron in the presence of a scalar potential. Baker shows that, in this approximation, the matrix element which must be evaluated is

$$M = \frac{k}{i} \int_0^\infty J_0(qb) \left[e^{i\chi(b)} - 1 \right] b \, db \tag{1}$$

where

$$\chi(b) = -\frac{E}{k} \int_{-\infty}^\infty V(b, z) dz \tag{2}$$

$$V(b, z) = V(r) = \int \rho(\vec{R}) V_c(|\vec{R} - \vec{r}|) d\vec{R} \tag{3}$$

Here $\rho(R)$ is the nuclear density function and $V_c(|\vec{R} - \vec{r}|)$ is the screened coulomb potential,

$$V_c(x) = -\frac{\alpha Z}{x} f\left(\frac{x}{a}\right)$$

where α is the fine structure constant, Z is the nuclear charge, and a is the screening radius, and the screening function used here is

$$f\left(\frac{x}{a}\right) = 1 - \frac{x}{\sqrt{x^2 + 4a^2}}$$

Assuming that the nuclear density is spherically symmetric, it can be shown that

$$\chi(b) = 8\pi\eta \int_0^\infty \rho(R) \int_0^\infty V_0(r, R) dz \, R^2 \, dR \tag{4}$$

where $r = \sqrt{b^2 + z^2}$, $V_0(r, R)$ is the zero order multipole of V_c, and $\eta = \alpha Z(E/k)$. Now $V_0(r, R)$ must be known only for values of $R \leq R_0$ under the assumption that $\rho(R)$ is negligibly small for $R > R_0$. Based on this assumption, it can be shown that

$$V_0(r, R) = \begin{cases} \dfrac{1}{r} f\left(\dfrac{r}{a}\right), & r \geq R \\[1em] R^{-1}, & r \leq R \end{cases} \tag{5}$$

Then it follows that

$$\chi(b) = \chi_0(b) + \chi_1(b) \tag{6a}$$

where

$$\chi_0(b) = \eta \, \log\left(1 + 4\,\dfrac{a^2}{b^2}\right) \tag{6b}$$

and

$$\chi_1(b) = 8\pi\eta \int_0^\infty dz \int_r^\infty \left(\dfrac{1}{R} - \dfrac{1}{r}\right)\rho(R)R^2 \, dR \tag{6c}$$

We have found it convenient to integrate equation (1) by parts, obtaining

$$M = \dfrac{k}{q} \int_0^\infty J_1(qb)\chi'(b)e^{i\chi(b)}b \, db \tag{7}$$

where $\chi'(b) = d\chi(b)/db$. The evaluation of $\chi_0'(b)$ is simple, and it can be shown that

$$\chi_1'(b) = \dfrac{8\pi}{b} \eta \int_0^\infty \rho\left(\sqrt{b^2 + r^2}\right)r^2 \, dr \tag{8}$$

This can then be integrated to obtain $\chi_1(b)$. Now, if we assume that $\rho(r)$ can be represented by a series of Gauss-Laguerre functions

$$\rho(R) = \sum_{n=0}^{\infty} A_n \mathscr{F}_n(\alpha, \beta r)$$

$$\mathscr{F}_n(\alpha, \beta r) = e^{-\alpha \beta^2 r^2} L_n^{1/2}(\beta^2 r^2)$$

$$(9)$$

and then make use of the addition theorem for Laguerre polynomials, it can be shown that

$$\rho\left(\sqrt{b^2 + r^2}\right) = e^{-\alpha \beta^2 b^2}\left[\rho(r) - (\beta b)^2 \sum_{m=1}^{\infty} \frac{L_{m-1}^1(\beta^2 b^2)}{m} \sum_{n=0}^{\infty} A_{m+n}\mathscr{F}_n(\alpha, \beta r)\right]$$

From this we obtain

$$\chi_1'(b) = \frac{2}{b}\eta e^{-\alpha \beta^2 b^2}\left[1 - 4\pi(\beta b)^2 \sum_{m=1}^{\infty} \frac{1}{m} L_{m-1}^1(\beta^2 b^2) B_m\right]$$

where

$$B_m \equiv \sum_{n=0}^{\infty} A_{m+n}D_n$$

and

$$D_n = \int_0^{\infty} \mathscr{F}_n(\alpha, \beta r)r^2\, dr$$

Equation (8) may be integrated to yield

$$\chi_1(b) = -2\eta \int_0^{\infty} e^{-\alpha \beta^2 R^2}\frac{dR}{R} + 4\pi\eta \sum_{m=1}^{\infty} I_{m-1}(\beta^2 b^2)B_m$$

$$I_m(x) = \int_x^{\infty} e^{-\alpha y}L_m^1(y)dy$$

The $\chi_0(b)$ and $\chi_1(b)$ and their derivatives are then used in equation (7) to obtain M. The final evaluation of the integral is carried out using the same general procedure as was used by Baker. The electron scattering form factor is related to the square of M divided by the point cross section. The change in the electron wavelength as the electron approaches the scattering center must be accounted for in the calculation of the form factor. The correction factor suggested by Ravenhall is used in our calculations (ref. 37).

REFERENCES

1. Ripka, Georges: The Hartree-Fock Theory of Deformed Light Nuclei. Advances in Nuclear Physics. Vol. 1. Michel Baranger and Erich Vogt, eds., Plenum Press, 1968, pp. 183-259.

2. Baranger, Michel: Theory of Finite Nuclei. 1962 Cargése Lectures in Theoretical Physics. Maurice Levy, ed., W. A. Benjamin, Inc., 1963, p. VI-89.

3. Yoshida, Shiro: Spectroscopic Study of Low Energy Vibrational States of Spherical Nuclei. Nucl. Phys., vol. 38, 1962, pp. 380-419.

4. Ford, William F.; and Braley, Richard C.: Hartree-Fock Calculations with Wood-Saxon Basis Functions. Nucl. Phys., vol. A134, 1969, pp. 265-276.

5. Gunye, M. R.: Effect of Truncation on the Projected Hartree-Fock Spectra. Nucl. Phys., vol. A128, 1969, pp. 457-464.

6. Ford, William F.; and Braley, Richard C.: E2 Transition Rates for ^{20}Ne. Nucl. Phys., vol. A126, 1969, pp. 671-674.

7. Bouten, M.; Bouten, M. C.; and Van Leuven, P.: Projected Hartree-Fock Calculations for Light Nuclei. (II). Form Factors of ^{6}Li. Nucl. Phys., vol. A100, 1967, pp. 105-112.

8. Sandhya Devi, K. R.; Khadkikar, S. B.; Parikh, J. K.; and Banerjee, B.: Projected Hartree-Fock-Bogolubov Calculation for the Ti Isotopes. Phys. Letters, vol. 32B, no. 3, June 22, 1970, pp. 179-181.

9. Braley, Richard C.; and Ford, William F.: Inelastic Scattering Calculations with Projected Hartree-Fock Wave Functions. Phys. Rev., vol. 182, no. 4, June 20, 1969, pp. 1174-1185.

10. Glendenning, Norman K.; and Veneroni, Marcel: Inelastic Scattering Based on a Microscopic Description of Nuclei. Phys. Rev., vol. 144, no. 3, Apr. 22, 1966, pp. 839-853.

11. Glendenning, Norman K.: Coupled Channel Treatment of Inelastic Scattering Based on Microscopic Nuclear Descriptions. Nucl. Phys., vol. A117, 1968, pp. 49-65.

12. Clement, David M.; and Baranger, Elizabeth U.: A Shell-Model Calculation of ^{18}F and ^{18}O Using the Tabakin Interaction. Nucl. Phys., vol. A108, 1968, pp. 27-48.

13. Shakin, C. M.; Waghmare, Y. R.; and Hull, M. H., Jr.: Unitary-Model-Operator Approach to Nuclear-Structure Physics. I. Phys. Rev., vol. 161, no. 4, Sept. 20, 1967, pp. 1006-1014.

24

14. Becker, Richard L.; MacKellar, Alan D.; and Morris, B. M.: Brueckner Theory in an Oscillator Basis. I. The Method of Reference Bethe-Goldstone Equations and Comparison of the Yale, Reid (Hard-Core), and Hamada-Johnston Interactions. Phys. Rev., vol. 174, no. 4, Oct. 20, 1968, pp. 1264-1290.

15. Gmitro, M.; and Sotona, M.: Brueckner Reaction Matrix and Separable Potentials. Phys. Rev., vol. C2, no. 2, Aug. 1970, pp. 356-365.

16. Castel, B.; and Parikh, J. C.: ^{28}Si Nucleus in the Projected Hartree-Fock Model. Phys. Rev., vol. C1, no. 3, Mar. 1970, pp. 990-994.

17. Tewari, S. N.; and Grillot, D.: Projected Hartree-Fock Spectrum of ^{28}Si Including Effects of Pairing and Shape Mixing. Phys. Rev., vol. 177, no. 4, Jan. 20, 1969, pp. 1717-1724.

18. Gunye, M. R.; and Warke, Chindhu S.: Projected Hartree-Fock Spectra of 2s-1d Shell Nuclei. Phys. Rev., vol. 156, no. 4, Apr. 20, 1967, pp. 1087-1093.

19. Giraud, B.; and Sauer, P. U.: Restoration of Rotational Symmetry for Triaxial Hartree-Fock Solutions. Phys. Letters, vol. 30B, no. 4, Oct. 13, 1969, pp. 218-220.

20. Bassichis, W. H.; Pohl, B. A.; and Kerman, A. K.: The Effects of Truncation in Nuclear Hartree-Fock Calculations. Nucl. Phys., vol. A112, 1968, pp. 360-371.

21. Braley, R. C.; Ford, W. F.; and Bar-Touv, J.: Basis States in Hartree-Fock Calculations. Bull. Am. Phys. Soc., vol. 14, no. 12, Dec. 1969, p. 1206.

22. Braley, Richard C.; Ford, William F.; and Bar-Touv, Jacob: Inelastic Scattering Calculations with Wood-Saxon Hartree-Fock Wavefunctions. Bull. Am. Phys. Soc., vol. 14, no. 4, Apr. 1969, p. 571.

23. Baker, Adolph: Relativistic High-Energy Approximation for Elastic Scattering of Dirac Particles. Phys. Rev., vol. 134, no. 1B, Apr. 13, 1964, pp. 240-251.

24. Glauber, R. J.: High-Energy Collision Theory. Lectures in Theoretical Physics. Vol. 1. Wesley E. Brittin and Lita G. Dunham, eds., Interscience Publ., 1959, pp. 315-414.

25. Bar-Touv, J.; and Goswami, A.: Inverted Coexistence of Spherical and Deformed States in Light Nuclei. Phys. Letters, vol. 28B, no. 6, Jan. 6, 1969, pp. 391-394.

26. Volkov, A. B.: Equilibrium Deformation Calculations of the Ground State Energies of 1p Shell Nuclei. Nucl. Phys., vol. 74, 1965, pp. 33-58.

27. Tabakin, Frank: An Effective Interaction for Nuclear Hartree-Fock Calculations. Ann. Phys. (N. Y.), vol. 30, no. 1, Oct. 20, 1964, pp. 51-94.

28. Nilsson, S. G.: Deformed Nuclei: Collective and Single Particle Aspects. Nuclear Structure Physics. Vol. VIIIC of Lectures in Theoretical Physics. P. D. Kunz, D. A. Lind, and W. E. Brittin, eds., University of Colorado Press, 1966, pp. 177-236.

29. Hill, David L.; and Wheeler, John A.: Nuclear Constitution and the Interpretation of Fission Phenomena. Phys. Rev., vol. 89, no. 5, Mar. 1, 1953, pp. 1102-1145.

30. Ford, William F.; and Braley, Richard C.: A Systematic Method of Calculating Reduced Matrix Elements of Single-Particle Operators. NASA TN D-5879, 1970.

31. Thompson, D. R.; and Tang, Y. C.: Resonating-Group Calculation for He^3-He^3 Scattering. Phys. Rev., vol. 159, no. 4, July 20, 1967, pp. 806-815.

32. Way, Katharine, ed.: Nuclear Data. Academic Press, 1965.

33. Bar-Touv, J.; Goswami, A.; Goodman, A. L.; and Struble, G. L.: Generalized Pairing in Light Nuclei. Phys. Rev., vol. 178, no. 4, Feb. 20, 1969, pp. 1670-1681.

34. Crawley, Gerard M.: Inelastic Proton Scattering in the 2s-1d Shell. Ph. D. Thesis, Princeton Univ., 1965.

35. Bar-Touv, J.; and Kelson, I.: Axially Asymmetric Regions in the 2s-1d Shell. Phys. Rev., vol. 138, no. 5B, June 7, 1965, pp. 1036-1041.

36. Harvey, M.; and Khanna, F. C.: Effective Operators in the Nuclear Shell Model. Nucl. Phys., vol. A152, 1970, pp. 588-608.

37. Helm, Richard H.: Inelastic and Elastic Scattering of 187-MeV Electrons from Selected Even-Even Nuclei. Phys. Rev., vol. 104, no. 5, Dec. 1, 1956, pp. 1466-1475.

TABLE I. - DESCRIPTION OF BASIS SPACES TO BE USED IN

HF CALCULATIONS

Radial dependence	Space	Basis
Harmonic oscillator	1	$(1s_{1/2}, 2s_{1/2}, 1d_{3/2}, 1d_{5/2}) (1p_{1/2}, 1p_{3/2})$
Harmonic oscillator	2	$(1s_{1/2}, 2s_{1/2}, 1d_{3/2}, 1d_{5/2})$ $(1p_{1/2}, 1p_{3/2}, 2p_{1/2}, 2p_{3/2}, 1f_{5/2}, 1f_{7/2})$
Harmonic oscillator	3	$(1s_{1/2}, 2s_{1/2}, 1d_{3/2}, 1d_{5/2}, 3s_{1/2}, 2d_{3/2}, 2d_{5/2}, 1g_{7/2}, 1g_{9/2})$. $(1p_{1/2}, 1p_{3/2}, 2p_{1/2}, 2p_{3/2}, 1f_{5/2}, 1f_{7/2})$
Wood-Saxon	--	$(1s_{1/2}, 2s_{1/2}, 1d_{3/2}, 1d_{5/2}) \cdot (1p_{1/2}, 1p_{3/2})$

27

TABLE II. - COMPARISON OF HF WAVE FUNCTIONS, SINGLE PARTICLE ENERGIES, HF ENERGIES, AND GAPS FOR NEON-20

[Oscillator length, 1.88 fm]

(a) HF wave functions and single particle energies

Magnetic quantum number m and parity π	Space (a)	Positive parity states									Single particle energy, e_λ, MeV
		$1s_{1/2}$	$2s_{1/2}$	$3s_{1/2}$	$1d_{3/2}$	$2d_{3/2}$	$1d_{5/2}$	$2d_{5/2}$	$1g_{7/2}$	$1g_{9/2}$	
		Negative parity states									
		$1p_{1/2}$	$2p_{1/2}$	$1p_{3/2}$	$2p_{3/2}$	$1f_{5/2}$	$1f_{7/2}$	-----	-----	-----	
$\frac{1}{2}^+$	1	0.9894	0.1336	-------	-0.0387	-------	0.0429	------	-------	------	-38.64
	2	0.9797	0.1890	-------	-0.0446	-------	0.0490	------	-------	------	-44.34
	3	0.9710	0.2156	0.0635	-0.0510	-0.0152	0.0566	0.0169	-0.0149	0.0120	-46.09
$\frac{1}{2}^-$	1	0.3173	-------	-0.9483	-------	-------	-------	------	-------	------	-19.16
	2	0.3249	0.0110	-0.9265	-0.1454	0.0766	-0.0942	------	-------	------	-23.08
	3	0.3536	0.0218	-0.9091	-0.1619	0.0947	-0.1130	------	-------	------	-24.21
$-\frac{3}{2}^-$	1	-------	-------	1.0000	-------	-------	-------	------	-------	------	-15.52
	2	-------	-------	0.9752	0.2145	0.0332	0.0432	------	-------	------	-18.43
	3	-------	-------	0.9687	0.2411	0.0363	0.0456	------	-------	------	-18.45
$\frac{1}{2}^-$	1	0.9483	-------	0.3173	-------	-------	-------	------	-------	------	-11.55
	2	0.9315	0.1235	0.3213	0.0879	0.0781	-0.0051	------	-------	------	-13.05
	3	0.9158	0.1429	0.3510	0.1033	0.0832	-0.0088	------	-------	------	-12.72
$\frac{1}{2}^+$	1	0.0212	-0.5062	-------	-0.3196	-------	0.8008	------	-------	------	-4.46
	2	0.0443	-0.5114	-------	-0.3165	-------	0.7977	------	-------	------	-6.06
	3	0.0468	-0.5016	-0.0417	-0.3577	-0.0109	0.7697	0.0637	-0.0788	0.1168	-7.96

[a]For definition of spaces see table I.

(b) HF energies and gaps

Basis	Energy, E_{HF}, MeV	Gap, Δ, MeV
1	-28.03	4.16
2	-36.85	5.36
3	-40.02	7.03

TABLE III. - PROJECTED RMS RADIUS AND

REDUCED E2 RATE

Basis	Oscillator length, b, fm	rms radius, $\langle R^2 \rangle^{1/2}$, fm	Transition rate, $B(E2;\ 0^+ \to 2^+)$, $e^2 \cdot fm^4$
Fixed oscillator length			
1	1.88	2.94	109.9
2	1.88	2.77	164.5
3	1.88	2.73	190.0
Fixed size of space			
3	1.82	2.68	174.7
	1.88	2.73	190.0
	1.93	2.78	204.1
Fixed rms radius			
1	1.78	[a]2.78	82.9
2	1.88	2.78	164.5
3	1.93	2.78	204.1

[a]Average of projected rms radii obtained with spaces and oscillator lengths shown. For spaces 1 and 3, values of $\langle R^2 \rangle^{1/2}$ are 2.79 and 2.77 fm, respectively. This introduces an uncertainty of about 2 percent in predicted E2 rates.

TABLE IV. - REDUCED E2 TRANSITION

RATES WITHIN GROUND STATE

BAND OF NEON-20

[Space, 3; oscillator length, 1.93 fm]

Transition	Predicted	Experiment
	Transition rate, $B(E2;\ J_i \to J_f)$, $e^2 \cdot fm^4$	
$0^+_1 \to 2^+_1$	204	286±15
$2^+_1 \to 4^+_1$	103	89±9
$4^+_1 \to 6^+_1$	90	129±13

TABLE V. - COMPARISON OF HF WAVE FUNCTIONS, SINGLE PARTICLE ENERGIES, HF ENERGIES,

GAPS, RMS RADII, AND E2 RATES FOR MAGNESIUM-24

[Oscillator length, 2.09 fm.]

(a) HF wave functions and single particle energies

Magnetic quantum number m and parity π	Space (a)	Positive parity states									Single particle energy, e_λ, MeV
		$1s_{1/2}$	$2s_{1/2}$	$3s_{1/2}$	$1d_{3/2}$	$2d_{3/2}$	$1d_{5/2}$	$2d_{5/2}$	$1g_{7/2}$	$1g_{9/2}$	
		Negative parity states									
		$1p_{1/2}$	$2p_{1/2}$	$1p_{3/2}$	$2p_{3/2}$	$1f_{5/2}$	$1f_{7/2}$	-------	-------	-------	
$\frac{1}{2}^{+}$	2	0.9745	0.2073	-------	-0.0554	-------	0.0662	-------	-------	-------	-39.94
	3	0.9621	0.2370	0.0672	-0.0686	-0.0311	0.0819	0.0354	-0.0045	0.0074	-44.14
$\frac{1}{2}^{-}$	2	-0.4061	-0.0515	0.8900	0.1741	-0.0521	0.0850	-------	-------	-------	-23.03
	3	-0.4356	-0.0772	0.8642	0.2037	-0.0726	0.1031	-------	-------	-------	-26.37
$-\frac{3}{2}^{-}$	2	-------	-------	-0.9655	-0.2413	-0.0597	-0.0773	-------	-------	-------	-17.41
	3	-------	-------	-0.9550	-0.2754	-0.0688	-0.0861	-------	-------	-------	-18.40
$\frac{1}{2}^{-}$	2	0.8884	0.1692	0.3948	0.1106	0.1064	0.0519	-------	-------	-------	-14.98
	3	0.8629	0.2002	0.4252	0.1295	0.1191	0.0594	-------	-------	-------	-15.69
$\frac{1}{2}^{+}$	2	0.0584	-0.5927	-------	-0.3024	-------	0.7442	-------	-------	-------	-7.40
	3	0.0479	-0.5398	-0.1227	-0.3341	-0.0323	0.7418	0.1267	-0.0511	0.0978	-10.14
$-\frac{3}{2}^{+}$	2	-------	-------	-------	-0.2823	-------	-0.9593	-------	-------	-------	-3.45
	3	-------	-------	-------	-0.2921	-0.0245	-0.9347	-0.1511	-0.0688	-0.1140	-4.56

[a]For definition of spaces see table I.

(b) HF energies and gaps

Basis	Energy, E_{HF}, MeV	Gap, Δ, MeV
2	-34.49	1.37
3	-40.87	1.70

(c) rms radii and E2 rates

Basis	rms radius, $\langle R^2 \rangle^{1/2}$, fm	$B(E2;\ 0_1^+ - 2_1^+)$, $e^2 \cdot fm^4$
2	3.20	351.9
3	3.037	373.9
Experiment	3.02±0.03	436±46

TABLE VI. - REDUCED E2 TRANSITION RATES WITHIN

GROUND STATE BAND OF MAGNESIUM-24

[Space 3; oscillator length, 2.09 fm.]

Transition	Predicted	Experiment
	Transition rate, $B(E2;\ J_i \rightarrow J_f)$, $e^2 \cdot fm^4$	
$0_1^+ - 2_1^+$	374	436±40
$2_1^+ - 4_1^+$	191	133±13

TABLE VII. – COMPARISON OF HF WAVE FUNCTIONS, SINGLE PARTICLE ENERGIES, HF ENERGIES, GAPS, RMS RADII, AND E2 RATES FOR SILICON-28 (OBLATE)

[Oscillator length, 2.09 fm.]

(a) HF wave functions and single particle energies

Magnetic quantum number m and parity π	Space (a)	Positive parity states $1s_{1/2}$ / Negative $1p_{1/2}$	$2s_{1/2}$ / $2p_{1/2}$	$3s_{1/2}$ / $1p_{3/2}$	$1d_{3/2}$ / $2p_{3/2}$	$2d_{3/2}$ / $1f_{5/2}$	$1d_{5/2}$ / $1f_{7/2}$	$2d_{5/2}$ / -------	$1g_{7/2}$ / -------	$1g_{9/2}$ / -------	Single particle energy, e_λ, MeV
$\frac{1}{2}^{+}$	2	0.9769	0.1946	-------	0.0566	-------	-0.0678	-------	-------	-------	-42.62
	3	0.9631	0.2365	0.0650	0.0631	0.0312	-0.0759	-0.0363	-0.0109	0.0111	-48.66
$-\frac{3}{2}^{-}$	2	-------	-------	-0.9772	-0.1842	0.0595	0.0868	-------	-------	-------	-24.86
	3	-------	-------	-0.9634	-0.2413	0.0679	0.0954	-------	-------	-------	-28.75
$\frac{1}{2}^{-}$	2	0.6328	0.0856	0.7461	0.1573	-0.0633	-0.0829	-------	-------	-------	-22.99
	3	0.6505	0.1335	0.7128	0.1935	-0.0755	-0.0885	-------	-------	-------	-26.59
$\frac{1}{2}^{-}$	2	0.7482	0.1395	-0.6171	-0.1701	-0.0927	0.0486	-------	-------	-------	-15.70
	3	0.7155	0.1782	-0.6350	-0.2039	-0.0955	0.0497	-------	-------	-------	-16.79
$\frac{5}{2}^{+}$	2	-------	-------	-------	-------	-------	1.000	-------	-------	-------	-8.78
	3	-------	-------	-------	-------	-------	0.9705	0.2145	0.0606	-0.0921	-11.66
$\frac{1}{2}^{+}$	2	-0.1059	0.7928	-------	-0.2375	-------	0.5512	-------	-------	-------	-7.82
	3	-0.1249	0.7356	0.1770	-0.2511	-0.0172	0.5730	0.1069	0.0451	-0.0824	-10.04
$-\frac{3}{2}^{+}$	2	-------	-------	-------	0.6893	-------	-0.7245	-------	-------	-------	-6.30
	3	-------	-------	-------	-0.6846	-0.1109	0.6950	0.1561	0.0562	0.0922	-8.51

(Negative parity state columns: $1p_{1/2}$, $2p_{1/2}$, $1p_{3/2}$, $2p_{3/2}$, $1f_{5/2}$, $1f_{7/2}$, -------, -------, -------)

a For definition of spaces see table I.

(b) HF energies and gaps

Basis	Energy, E_{HF}, MeV	Gap, Δ, MeV
2	-50.30	5.31
3	-61.16	7.24

(c) rms radii and E2 rates

Basis	rms radius, $\langle R^2 \rangle^{1/2}$, fm	$B(E2; 0_1^- - 2_1^-)$, $e^2 \cdot fm^4$
2	3.336	438.9
3	3.096	376.2
Experiment	3.08±0.06	327·17

TABLE VIII. - COMPARISON OF RMS RADIUS RADIUS AND REDUCED

E2 RATES FOR SILICON-28

[Oscillator length, 2.09 fm.]

Description	rms radius, $\langle R^2 \rangle^{1/2}$, fm	Transition rate, $e^2 \cdot fm^4$	
		$B(E2; 0_1^+ - 2_1^+)$	$B(E2; 0_2^+ - 2_1^+)$
Oblate	3.096	376.2	----
Inverted co-existence calculation	3.092	342.3	34.2
Experiment	3.08±0.06	327±17	35±4

TABLE IX. - COMPARISON OF HF WAVE FUNCTIONS, SINGLE PARTICLE ENERGIES, HF ENERGIES, GAPS, PROJECTED RMS RADIUS, AND E2 RATES FOR SULFUR-32 (PROLATE)

[Oscillator length, 2.19 fm.]

(a) HF wave functions and single particle energies

Magnetic quantum number m and parity π	Space (a)	Positive parity states $1s_{1/2}$ / Negative parity states $1p_{1/2}$	$2s_{1/2}$ / $2p_{1/2}$	$3s_{1/2}$ / $1p_{3/2}$	$1d_{3/2}$ / $2p_{3/2}$	$2d_{3/2}$ / $1f_{5/2}$	$1d_{5/2}$ / $1f_{7/2}$	$2d_{5/2}$	$1g_{7/2}$	$1g_{9/2}$	Single particle energy, e_λ, MeV
$\frac{1}{2}^+$	2	0.9783	0.1982	-------	0.0372	-------	-0.0476	-------	-------	-------	-41.22
	3	0.9617	0.2540	0.0684	0.0432	0.0240	-0.0536	-0.0262	-0.0021	0.0014	-48.95
$-\frac{3}{2}^-$	2	-------	-------	-0.9773	-0.2038	0.0308	0.0485	-------	-------	-------	-24.52
	3	-------	-------	-0.9581	-0.2786	0.0369	0.0554	-------	-------	-------	-29.59
$\frac{1}{2}^-$	2	0.6130	0.1013	0.7635	0.1636	-0.0277	-0.0590	-------	-------	-------	-22.62
	3	0.6568	0.1706	0.7017	0.2051	-0.0386	-0.0598	-------	-------	-------	-27.27
$\frac{1}{2}^-$	2	0.7652	0.1514	-0.5981	-0.1594	-0.0695	0.0602	-------	-------	-------	-18.66
	3	-0.7010	-0.2039	0.6415	0.2143	0.0724	-0.0658	-------	-------	-------	-21.53
$\frac{5}{2}^+$	2	-------	-------	-------	-------	-------	1.000	-------	-------	-------	-9.06
	3	-------	-------	-------	-------	-------	0.9621	0.2665	0.0298	-0.0498	-12.38
$\frac{1}{2}^+$	2	-0.1336	0.8203	------	-0.1865	-------	0.5234	-------	-------	-------	-7.99
	3	-0.1668	0.7393	0.2238	-0.1911	-0.0295	0.5633	0.1327	0.0199	-0.0533	-10.47
$-\frac{3}{2}^+$	2	-------	-------	-------	0.5437	-------	-0.8392	-------	-------	-------	-7.08
	3	-------	-------	-------	0.5557	0.1290	-0.7912	-0.2088	-0.0146	0.0683	-9.64
$-\frac{3}{2}^+$	2	-------	-------	-------	-0.8392	-------	-0.5437	-------	-------	-------	-4.68
	3	-------	-------	-------	-0.8003	-0.1727	-0.5523	-0.1311	0.0683	0.0535	-6.09

[a] For definition of spaces see table I.

(b) HF energies and gaps

Basis	Energy, E_{HF}, MeV	Gap, Δ, MeV
2	-51.3	0.71
3	-64.74	1.02

(c) Projected rms radius and E2 rates

Basis	rms radius, $\langle R^2 \rangle^{1/2}$, fm	$B(E2; 0_1^+ - 2_1^+)$,
2	3.567	401.9
3 (prolate)	3.240	325.1
3 (oblate)	3.246	244.2
Experiment	3.23±0.07	217±30

Magnetic quantum number m and parity π	Basis	$1s_{1/2}$	$2s_{1/2}$	$1d_{3/2}$	$1d_{5/2}$	$1p_{1/2}$	$1p_{3/2}$	Single particle energy, e_λ, MeV
$\frac{1}{2}^+$	WS	0.9969	0.0718	-0.0196	0.0249	-------	-------	-57.95
	HO	0.9881	0.1436	-0.0345	0.0422	-------	-------	-47.69
$\frac{1}{2}^-$	WS	-------	-------	-------	-------	-0.4253	0.9051	-28.10
	HO	-------	-------	-------	-------	-0.5774	0.8165	-25.13
$-\frac{3}{2}^-$	WS	-------	-------	-------	-------	-------	-1.0000	-23.39
	HO	-------	-------	-------	-------	-------	-1.0000	-19.17
$\frac{1}{2}^-$	WS	-------	-------	-------	-------	0.9051	0.4253	-21.63
	HO	-------	-------	-------	-------	0.8165	0.5774	-19.17
$\frac{1}{2}^+$	WS	-0.0279	0.7009	0.4760	-0.5305	-------	-------	-6.10
	HO	0.0346	-0.5540	-0.5261	0.6443	-------	-------	-9.97

TABLE XI. - COMPARISON OF NUCLEAR PROPERTIES WITH

HARMONIC OSCILLATOR (HO) AND WOOD-SAXON (WS) BASIS

[Oscillator length, 1.924 fm.]

Nucleus	Basis	rms radius, $R^{2^{1/2}}$ fm	Transition rate, B(E2; $0^+ - 2^+$), $e^2 \cdot fm^4$	Energy, E_{HF}, MeV	Gap, Δ, MeV
^{20}Ne	HO	3.01	135.7	-98.37	8.33
	WS	2.84	140.8	-84.98	8.04
^{24}Mg	HO	3.12	191.2	-116.77	0.24
	WS	2.96	174.4	-87.54	0.11
^{28}Si	HO	3.20	269.8	-160.15	9.11
	WS	3.09	274.9	-116.03	8.62
^{32}S	HO	3.25	192.8	-193.75	0.24
	WS	3.17	182.7	-134.15	0.22
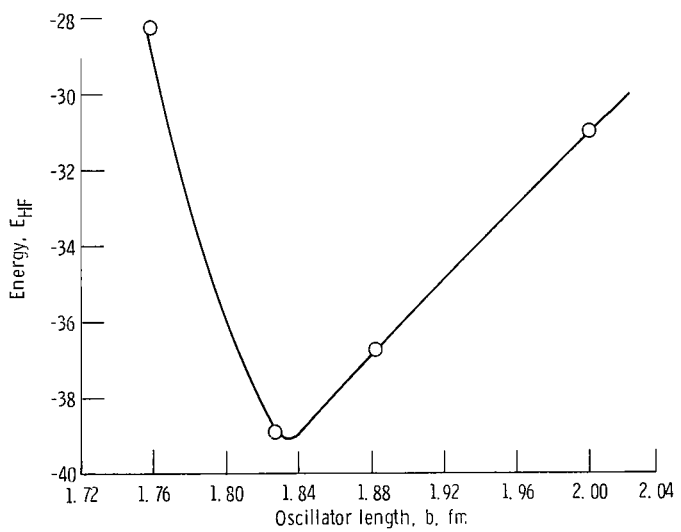
Figure 1. - Plot of HF energy as function of oscillator length for neon-20 (space, 2).
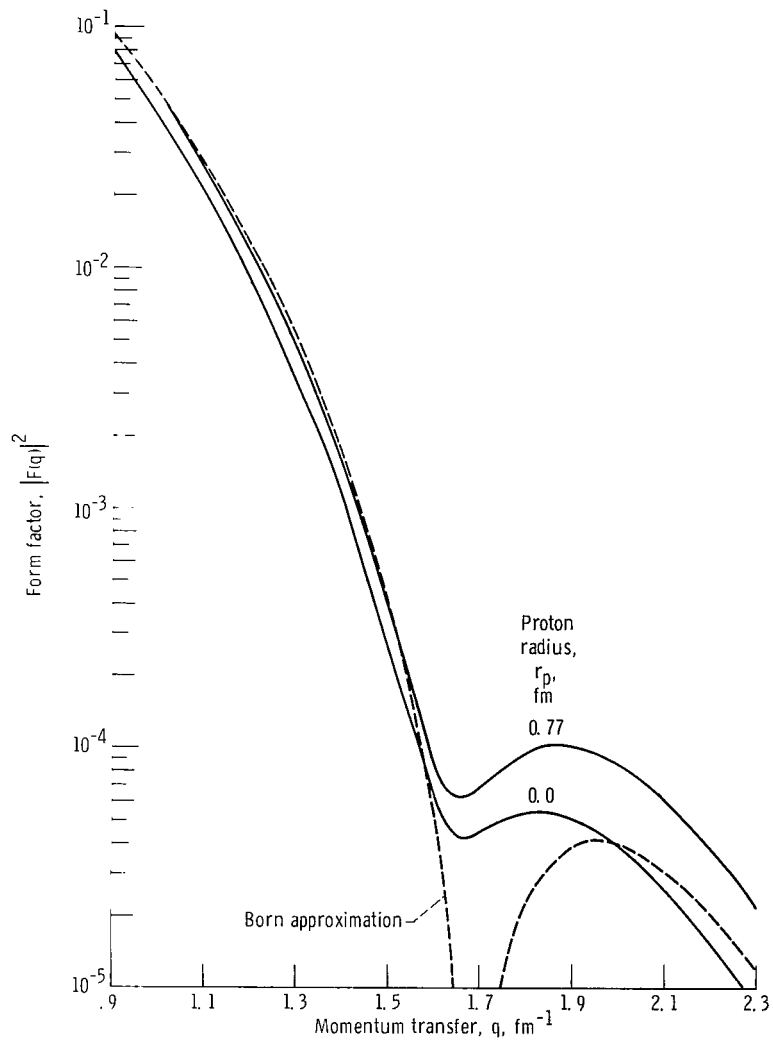
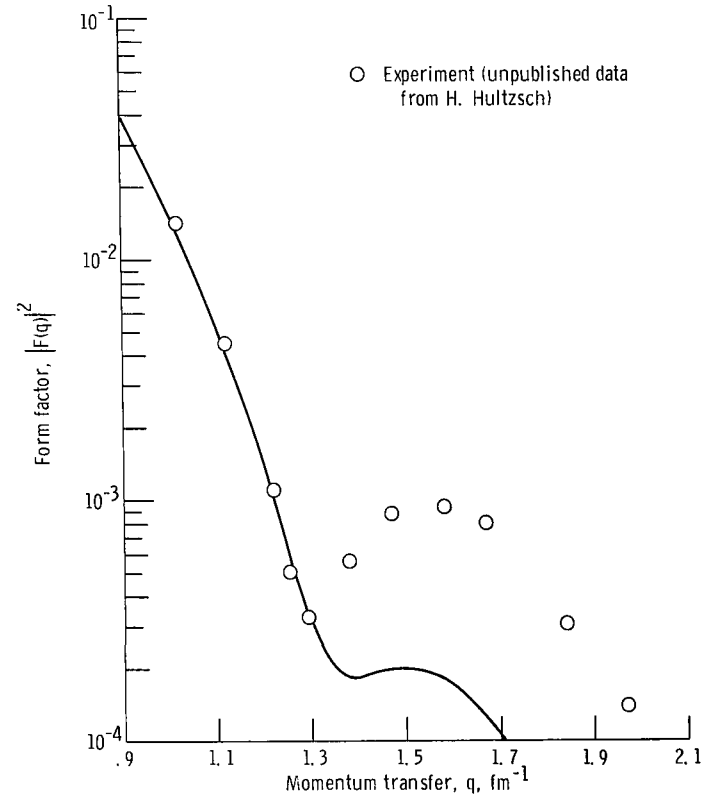Figure 2. - Neon-20 elastic form factor for 200-MeV electrons. Oscillator length, 1.93 femtometers; basis space, 3.
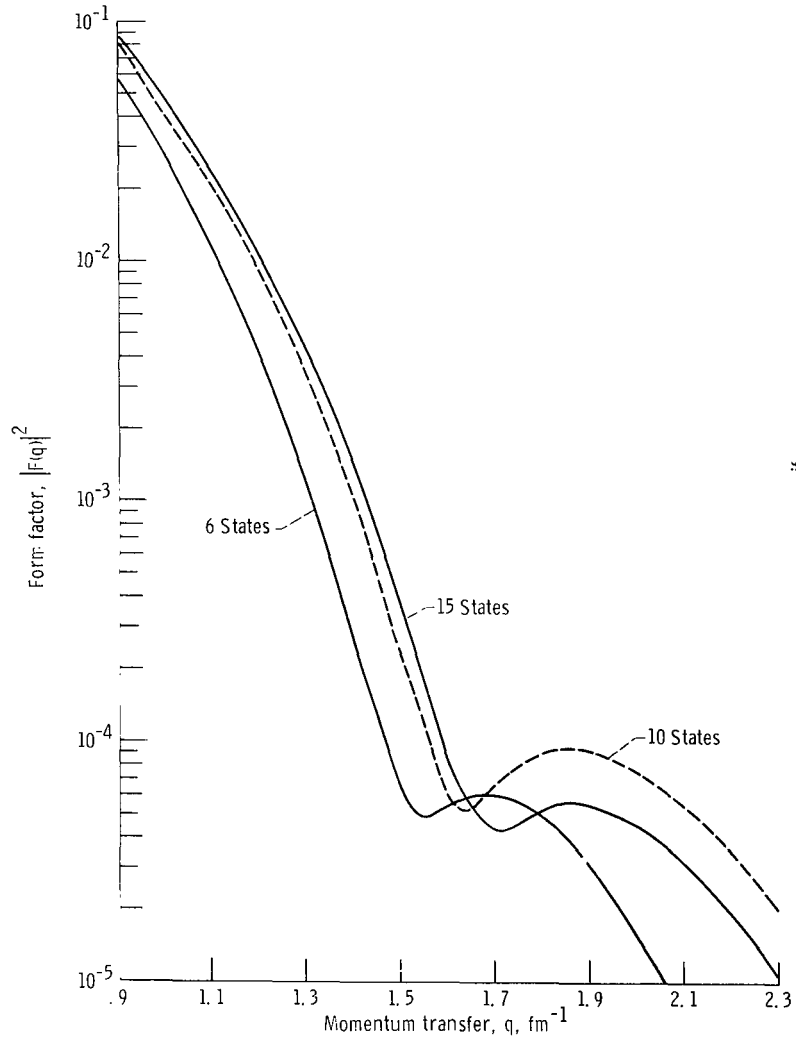
Figure 3. - Neon-20 elastic form factor for 200-MeV electrons. Comparison for 6, 10, and 15 state spaces. Proton radius, 0.77 femtometers.
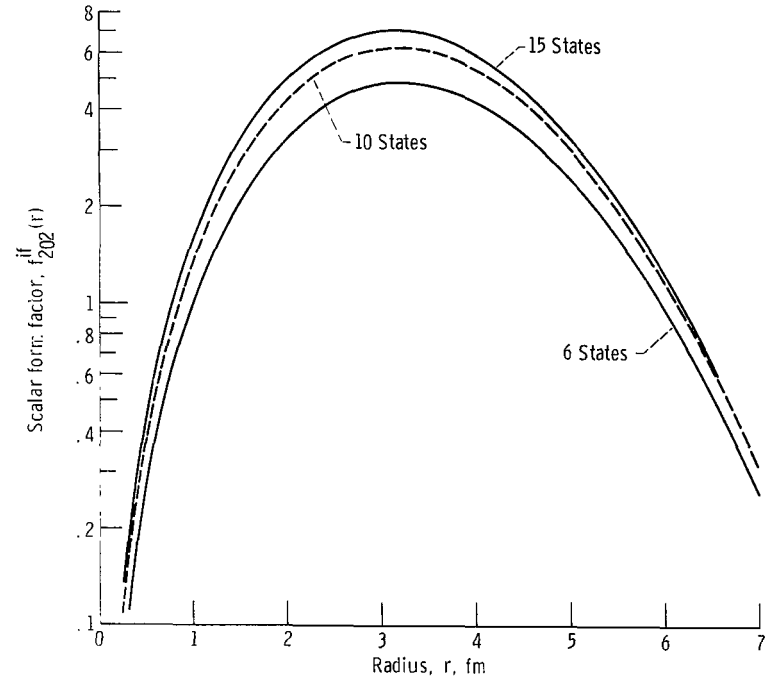
Figure 4. - Neon-20 scalar form factor. (LSJ = 202.)
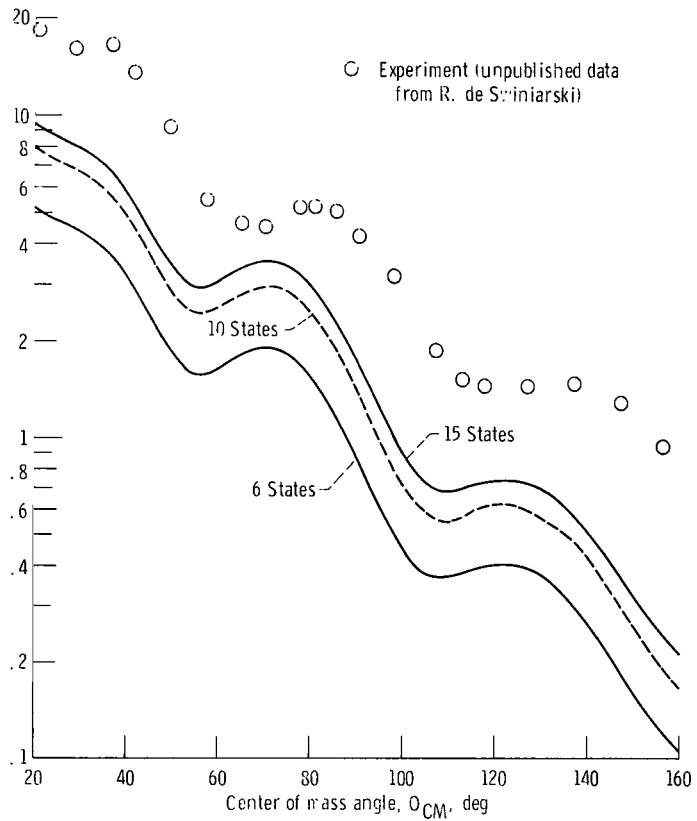
Figure 5. - Predicted inelastic cross sections for proton scattering compared with experiment for three spaces. Oscillator length, 1.88 femtometers; proton lab energy 24.5 MeV; Q-value, 1.63 (2+).
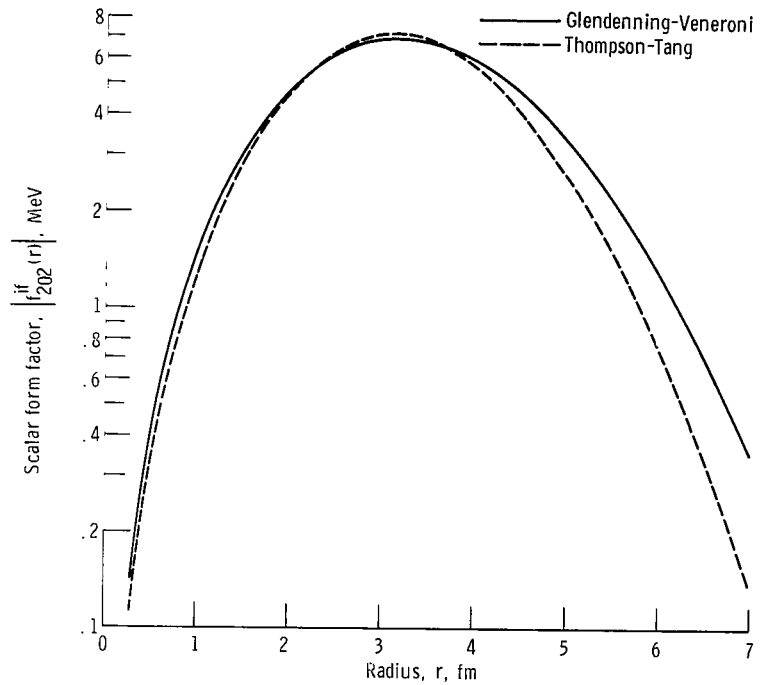
Figure 6. - Neon-20 scalar form factor. (LSJ = 202.)
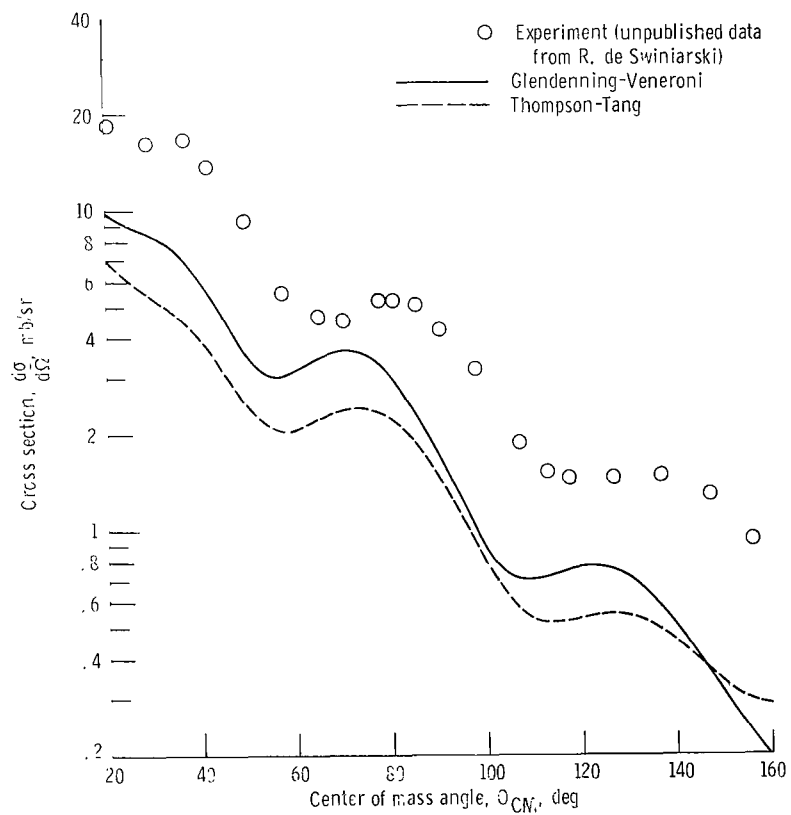
Figure 7. - Predicted angular distribution for inelastic proton scattering compared with experiment using form factors from neon-20 from figure 6.   Proton lab energy, 24.5 MeV, Q-value, -1.63 MeV (2⁺).
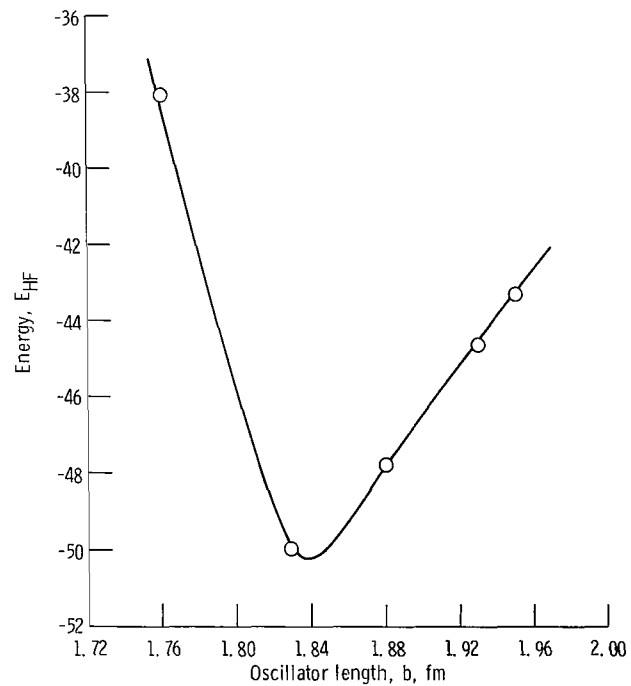
Figure 8. - Plot of HF energy as function of oscillator length for magnesium-24.   Ten state space.
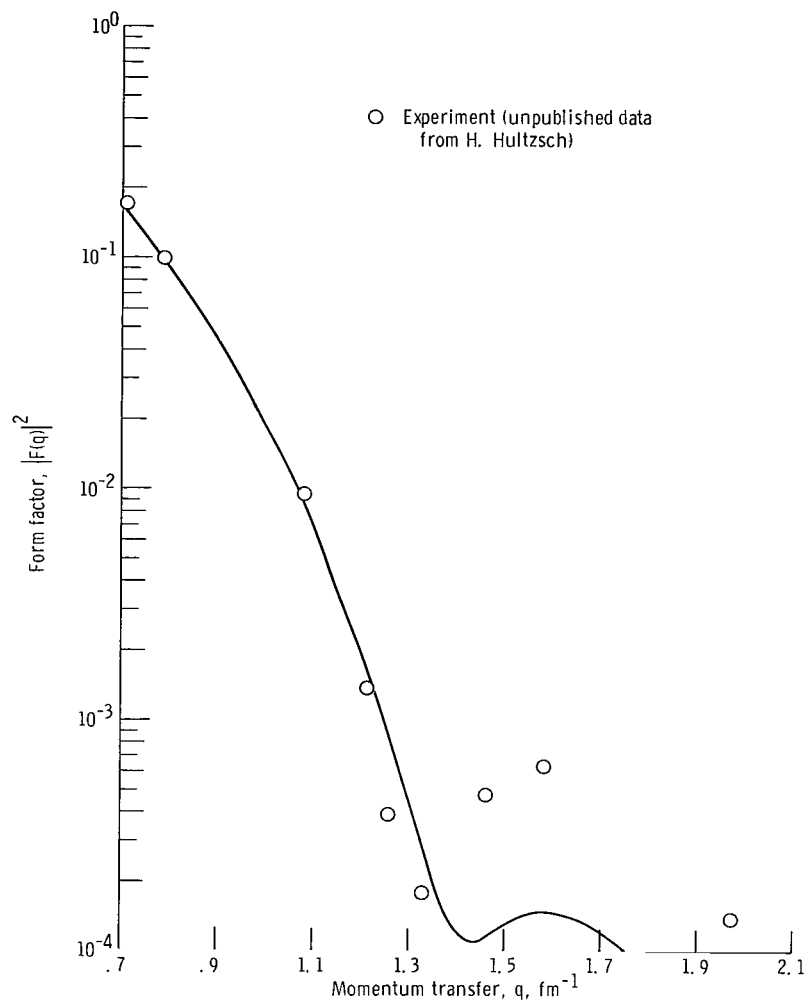
Figure 9. - Magnesium-24 elastic form factor for 189-MeV electrons. Oscillator length, 2. 09 femtometers.
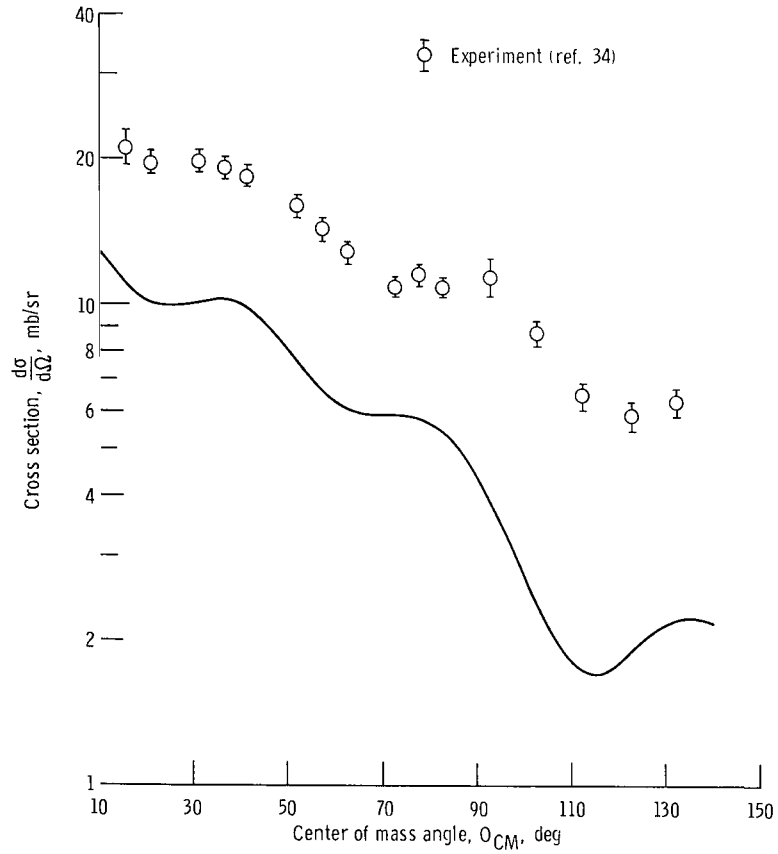
Figure 10. - Predicted angular distributions for inelastic proton scattering from magnesium-24 compared with experiment for 15 state space. Oscillator length, 2.09 femtometers; proton lab energy, 17.5 MeV; Q-values, 1.37 MeV (2^+).

Figure 11. - Silicon-28 elastic form factor for 240-MeV electrons. Oscillator length, 2.09 femtometers; basis space, 3.
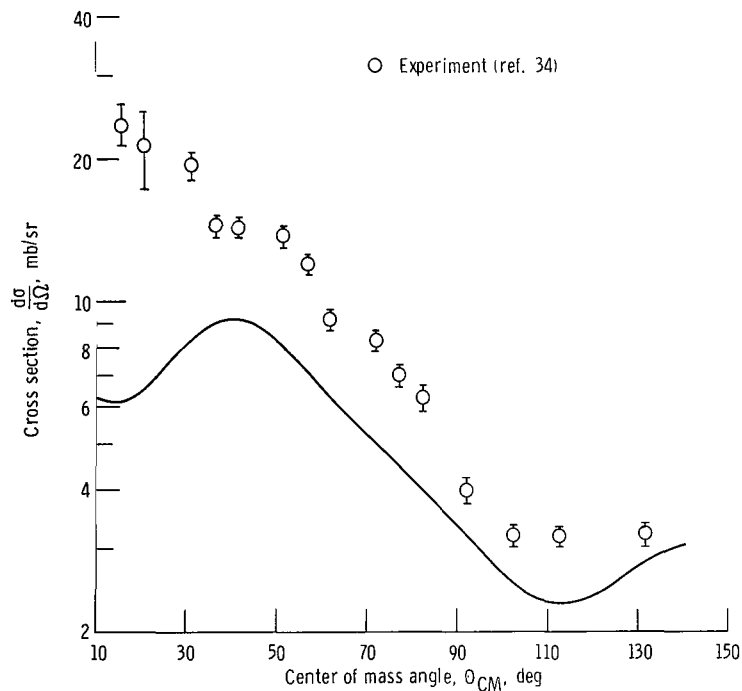
Figure 12. - Predicted angular distribution for inelastic proton scattering from silicon-28 compared with experiment. Oscillator length, 2.09 femtometers; basis space, 3; proton lab energy, 17.5 MeV; Q-value, -1.78 MeV (2^+).
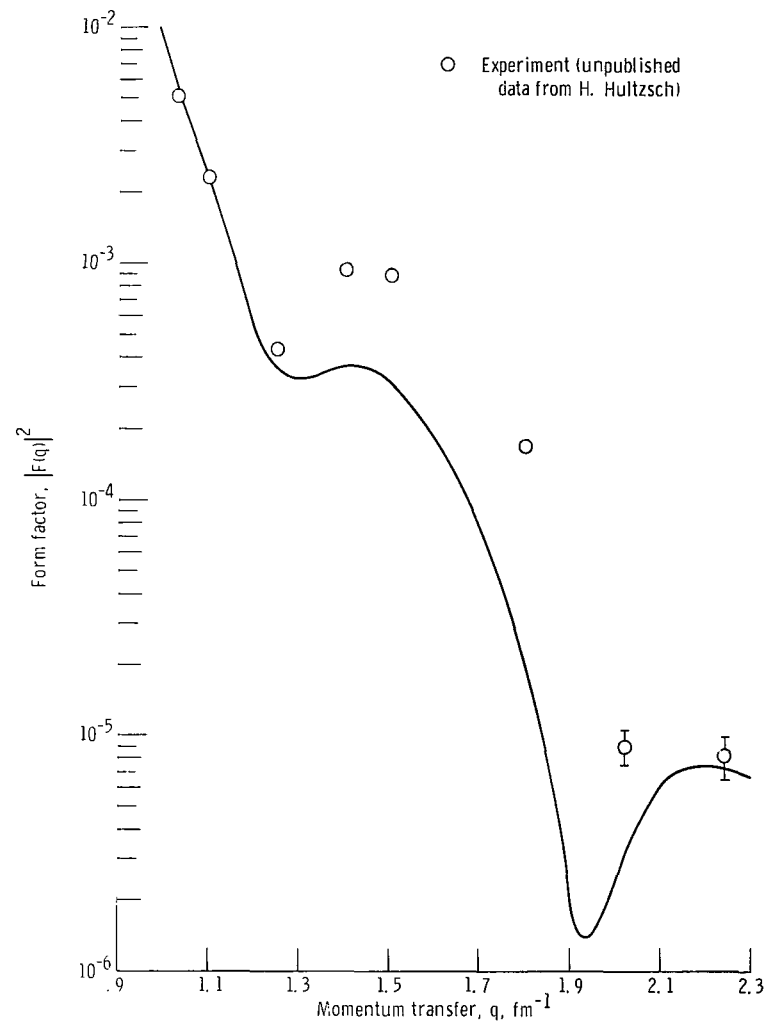
Figure 13. - Sulfur-32 elastic form factor for 262-MeV electrons. Oscillator length, 2.49 femtometers; basis space, 3.
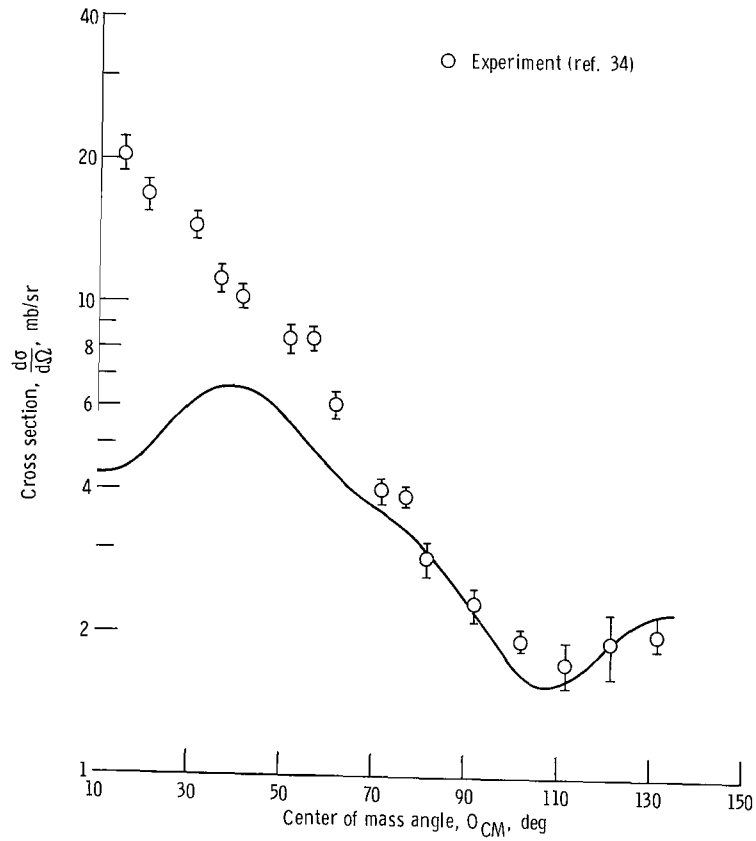
Figure 14. - Predicted angular distribution for inelastic proton scattering from sulfur-32 compared with experiment. Oscillator length, 2.19 femtometers; basis space, 3; proton lab energy, 17.5 MeV; Q-value, -2.24 MeV (2$^+$).
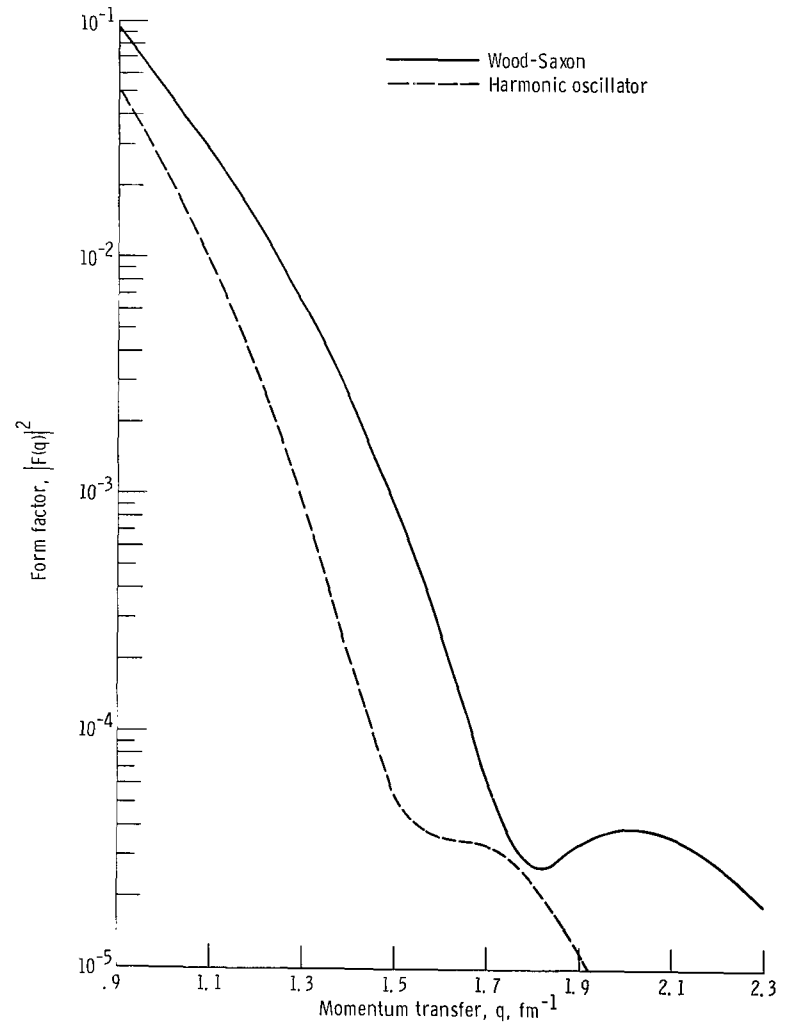
Figure 15. - Comparison of elastic form factors for neon-20 using Wood-Saxon and harmonic oscillator bases with 6 states.
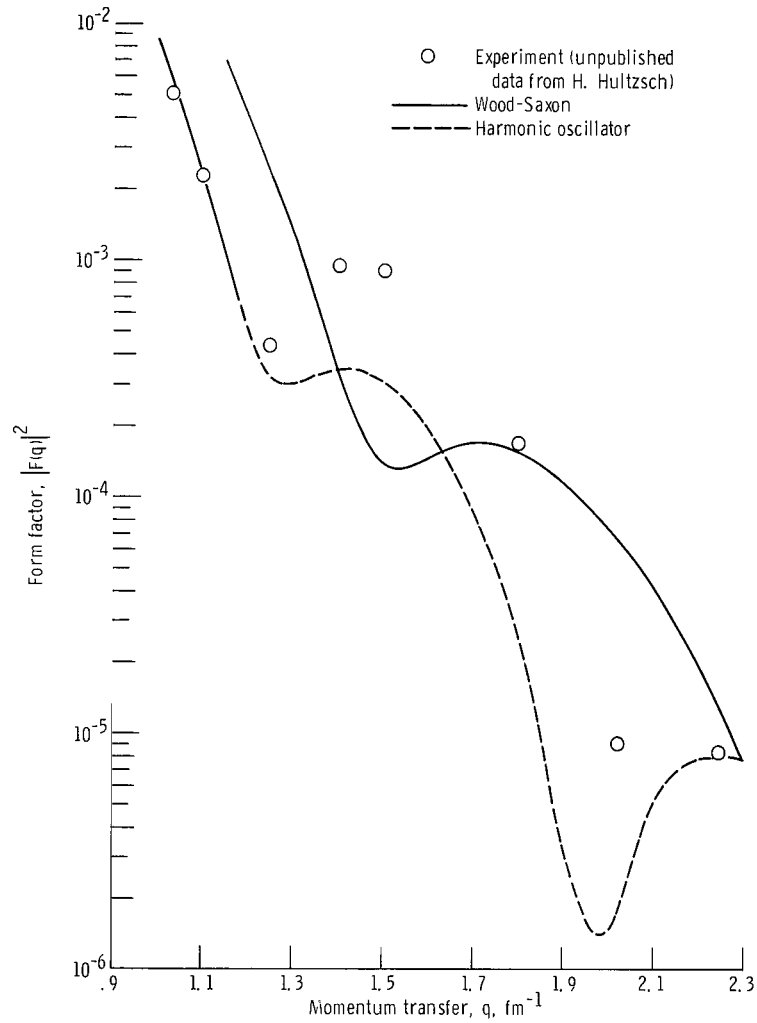
Figure 16. – Comparison of elastic form factors for sulfur-32 using Wood–Saxon and harmonic oscillator bases with 6 states. Energy, 262 MeV.
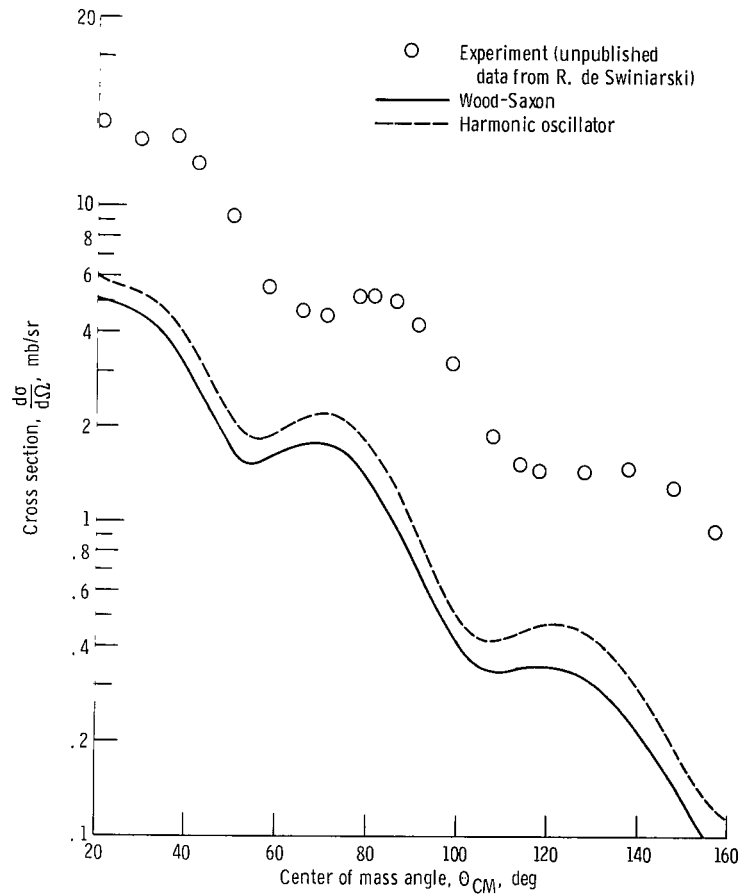
Figure 17. – Predicted angular distributions for inelastic proton scattering from neon-20 compared with experiment using Wood–Saxon and harmonic oscillator bases with 6 states. Proton lab energy, 24.5 MeV; Q-value, -1.63 MeV (2+).
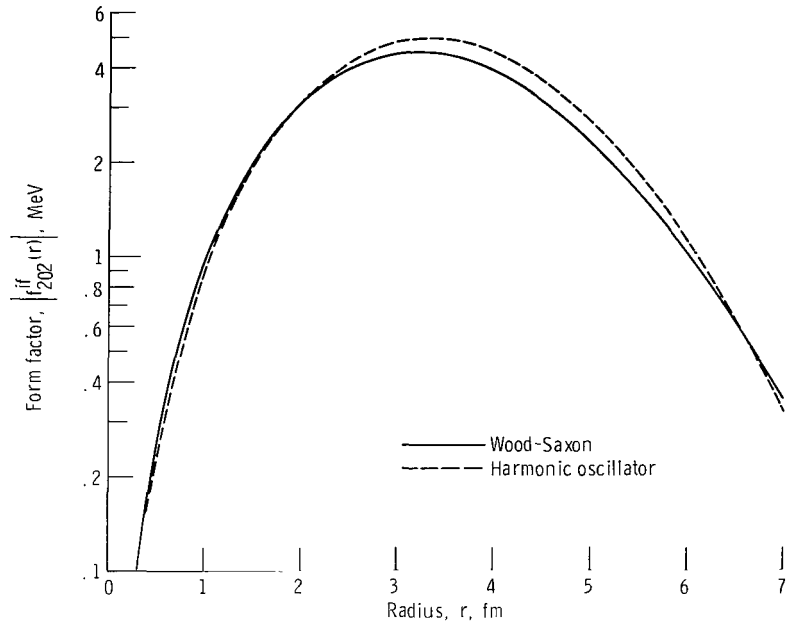
Figure 18. - Comparison of scalar form factors for neon-20 with 6 state Wood-Saxon and harmonic oscillator model spaces. (LSJ = 202.)
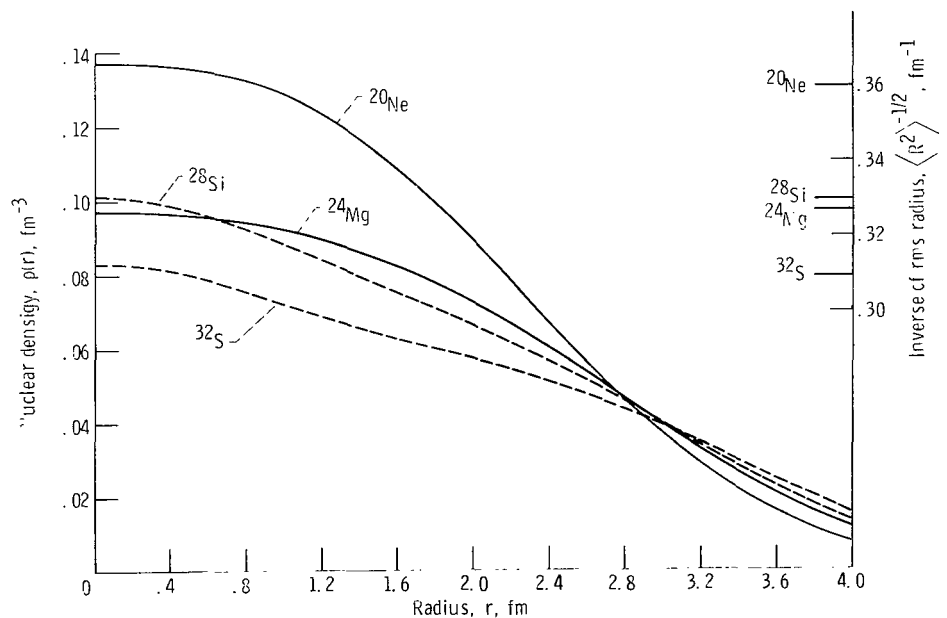
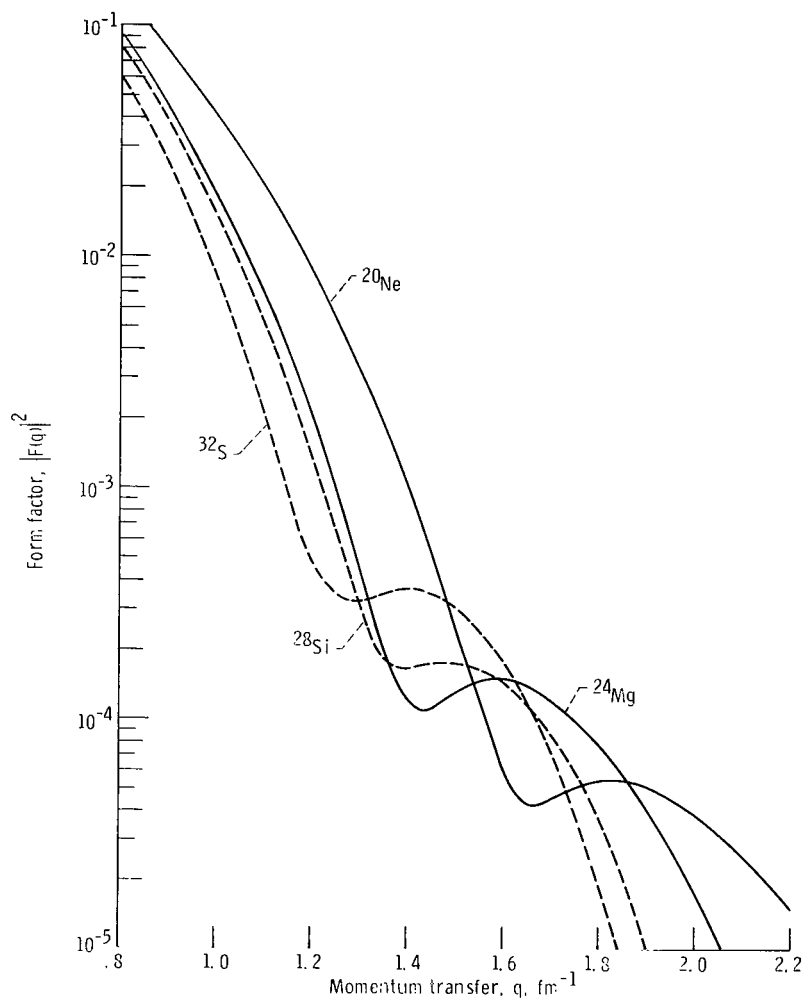Figure 19. - Nuclear density as function of radius for 15 state bases.

44

Figure 20. - Elastic electron form factors corresponding to densities in figure 19.

"*The aeronautical and space activities of the United States shall be conducted so as to contribute . . . to the expansion of human knowledge of phenomena in the atmosphere and space. The Administration shall provide for the widest practicable and appropriate dissemination of information concerning its activities and the results thereof.*"

— NATIONAL AERONAUTICS AND SPACE ACT OF 1958

NASA SCIENTIFIC AND TECHNICAL PUBLICATIONS

TECHNICAL REPORTS: Scientific and technical information considered important, complete, and a lasting contribution to existing knowledge.

TECHNICAL NOTES: Information less broad in scope but nevertheless of importance as a contribution to existing knowledge.

TECHNICAL MEMORANDUMS: Information receiving limited distribution because of preliminary data, security classification, or other reasons.

CONTRACTOR REPORTS: Scientific and technical information generated under a NASA contract or grant and considered an important contribution to existing knowledge.

TECHNICAL TRANSLATIONS: Information published in a foreign language considered to merit NASA distribution in English.

SPECIAL PUBLICATIONS: Information derived from or of value to NASA activities. Publications include conference proceedings, monographs, data compilations, handbooks, sourcebooks, and special bibliographies.

TECHNOLOGY UTILIZATION PUBLICATIONS: Information on technology used by NASA that may be of particular interest in commercial and other non-aerospace applications. Publications include Tech Briefs, Technology Utilization Reports and Technology Surveys.

Details on the availability of these publications may be obtained from:

SCIENTIFIC AND TECHNICAL INFORMATION OFFICE

NATIONAL AERONAUTICS AND SPACE ADMINISTRATION
Washington, D.C. 20546